CODEN:LUTEDX/(TEIE-5361)/1-94/(2015)

Industrial Electrical Engineering and Automation

Design Evaluation of a High Voltage High Frequency Pulse Transformer

Dmitri Ivanov

Division of Industrial Electrical Engineering and Automation
Faculty of Engineering, Lund University

LTH

IEA

Design Evaluation of a HVHF Pulse Transformer

Author:
Dmitri Ivanov

Supervisor:
Avo Reinap

Spring Semester 2015

Abstract

Unlike commonly used regular transformers, high voltage, high frequency, pulsed transformers are generally represented in special purpose applications. This often means that these electrical devices must be tailored in accordance with the specific requirements of the project. The pulse transformer under analysis in this thesis is a prototype machine variation of which will serve as an essential part of klystron feeder system at the European Spallation Source.

In the given application hundreds of pulse transformers will be required in order to supply power for the particle accelerator. The devices will be be integrated into high voltage, high frequency, pulsed power modules. The importance of careful analysis of the prototype system can therefore not be stressed enough.

Throughout this thesis work the reliability and functionality of the prototype pulse transformer are examined closely with help of analytic methods, computer aided simulation and laboratory analysis. The design is evaluated in terms of several important qualities such as low voltage drop, sufficient rise times and ability to operate without occurrence of unwanted high voltage phenomena. Both electromagnetic and mechanic aspects are included into the study.

As the result of the performed work, an evaluation conclusion is presented together with possible improvements of the current design. Aim of the study is to provide a verification as well as present possible alternatives for the transformer system design.

Acknowledgments

First of all I would like to thank my supervisor, Avo Reinap, for his guidance, support and patience throughout this thesis project. I thank Carlos Martins, Göran Göransson and Getachew Darge for introducing me to the work at hand and supporting me throughout the semester. I also thank Gabriel Domingues, Lars Lindgren, Jonas Johansson, Max Collins, Finn Landegren and Sebastian Hall both for their invaluable inputs and for making my stay at the department highly enjoyable. I thank Johannes Kazantzidis for reviewing this report and for useful advice. Finally I want to thank my friends, family and Hanna Andersson for general support throughout the thesis work.

List of Abbreviations

HV	High Voltage
HF	High Frequency
ESS	European Spallation Source
CAD	Computer-aided Design
Primary	Primary, low voltage winding of the transformer
Secondary	Secondary, high voltage winding of the transformer
PCB	Printed Circuit Board
RF	Radio Frequency
2D	Two Dimensional
3D	Three Dimensional
FEM	Finite Element Method
CMC	Common Mode Choke
AC	Alternating Current
DC	Direct Current

List of Figures

List of Tables

Contents

1 Introduction

Pulse transformers are electrical devices used to increase or decrease the voltage provided by an external pulsed source. In most ways their appearance and function are closely related to those of conventional transformers. However steep flanks of the pulses are typically associated with high frequency components, making pulse transformers and their design process partially similar to high frequency transformers. The design considerations therefore include concerns regarding saturation behavior and oscillations during the pulse, efficiency at different load points as well as enhancement of rise time.

The transformer under analysis is a prototype entity which is developed with the purpose of testing a design that later is to be implemented as a part of klystron feeder system at the European Spallation Source.

The task of the machine and its subsystems is to transform 1 kV peak-to-peak 15 kHz signal, pulsed at 14 Hz in 3.5 ms long pulses to 25 kHz uniform pulses. Due to each klystron feeder containing six 25 kV systems connected in series an insulation requirement of 150 kV is imposed on the transformer. A further requirement is an insulation of 25 kV for each of the subsystems.

In order for the prototype to serve as a template for further large scale manufacturing process it is necessary to closely analyze its functionality and consider improvements to the design.

1.1 Background

The pulse transformer, which lies at the core of this thesis work is a part of a larger HV power supply system being developed for the European Spallation Source. The purpose of each system is to provide pulsed power to a klystron, around one hundred of these will be deployed in the accelerator tunnel of the ESS. Klystrons are linear beam tubes where an oscillating electric field is applied to a beam of charged particles. A fraction of the particles are accelerated and the resulting beam then consists both of initial dc component and a nonsinusoidal ac component. The beam then travels into consequtive cavities where it induces RF currents which enhance the velocity modulation of the beam. The process results in a higher RF power being obtained at the output of the klystron than its input. The charged particles to be accelerated at ESS will be protons.

After attaining the required RF power the beam will be used to release neutrons through spallation by hitting a target consisting of tungsten.

A fraction of the neutrons released by the collision are then projected at material or device under analysis.

1.2 Objective

The primary objective of this thesis is to evaluate the provided HVHF transformer prototype, including the closest subsystems, in terms of their ability to provide specified pulsed power under load, but also in terms their geometrical design as well as other design choices such as HV isolation and parameters affecting the magnetic and electrostatic qualities of the transformer. The evaluation process is documented and the results used as basis for possible improvements to the system.

1.3 Method

Initially a literature study is made, including articles and books on transformer design, electromagnetic field theory and high voltage systems.

An evaluation of the device is then performed using system analysis. In order for the analysis to produce reliable results, parameter and component values are acquired using several techniques in parallel. These include analytic modeling, modeling using finite element software, notably FEMM and Comsol as well as practical evaluation performed using the transformer prototype.

Results of different analysis strategies are then examined and tested on a system level. Once weak points of the design are identified, variable parameters of the system are adjusted and the evaluation is performed again, resulting in an iterative process presenting various design options for the transformer.

1.4 Limitations

Due to time constraints, several important planes of analysis are by necessity omitted. In the physical sphere these include thermal analysis of the system and electrostatic analysis of the subsystems.

From an industrial point of view no thorough analysis is presented when it comes to cost efficiency, construction difficulties and production process.

A number of laboratory system tests are not performed due to transformer or the feeding system being under construction and testing by other groups. Overall, the transformer and the subsystems being under continuous development somewhat hindered the analysis due to continuous need of updating the models.

2 System Overview

In this chapter an introduction is made to the final design of the prototype transformer, which is at the moment of writing under testing at the IEA department of LTH. A brief introduction will also be made to subsystems relevant for the requirements on, and overall functionality of the transformer.

Due to geometrical and physical evaluations performed in later chapters it is advantageous to get a clear picture of the complete design before moving on to the analysis itself.

It is also important to notice that parameters presented in this chapter are only partially provided by the manufacturers, a number of values that were not available were instead acquired through measurements or approximations. During the project it has become apparent that a considerable number of parameters needed for analysis are either not provided by the suppliers or are presented in the documentation, but do disagree with reality to some extent. Whenever uncertain parameters are used, or replaced with a more fitting ones throughout the project there will be comments regarding the choice of the new data.

2.1 System Components

While the transformer is at the center of attention in this report, it is necessary to consider subsystems and components, which affect its function and play an essential role in understanding the requirements that are imposed on the system, and therefore the transformer itself. Main subsystems in the same cluster are common mode choke, rectifier bridge and a filter inductor. All of these, together with the transformer reside in common oil tank. Below, in Figure 1 a schematic overview of the system is presented.

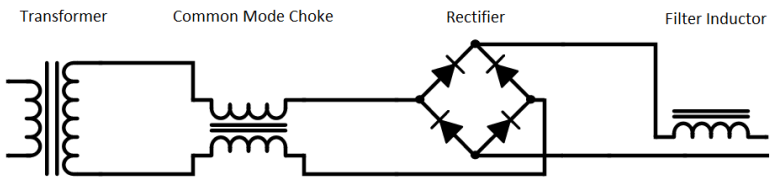

Figure 1: Schematic layout of the system. From left to right: transformer, common mode choke, rectifier, filter inductor

The main task of the transformer is to step-up transform 1 kV pulses to 25 kV with smallest possible voltage drop and with low overshoot and oscillations. The pulse train consist of a 3.5 ms long envelopes pulsed at a frequency of 14 Hz, the envelopes themselves contain 15 kHz square wave.

The common mode choke is implemented in order to protect the transformer from common mode currents coming from the HV side of the system. These are not expected to surpass 0.1 A. The common mode signals passing the component are attenuated.

The rectifier is a diode bridge which provides full wave rectification of the 15 kHz, 25 kV waveform provided by the transformer.

Filter Inductor is the final system step, responsible for filtering the output of the rectifier. This is needed due to high-frequent voltage ripple at the output of the system.

Below, in Figure 2 a full system model is shown. Note that both the common mode choke and the rectifier consists of multiple components. A thorough description of each system component is presented further on in this chapter.

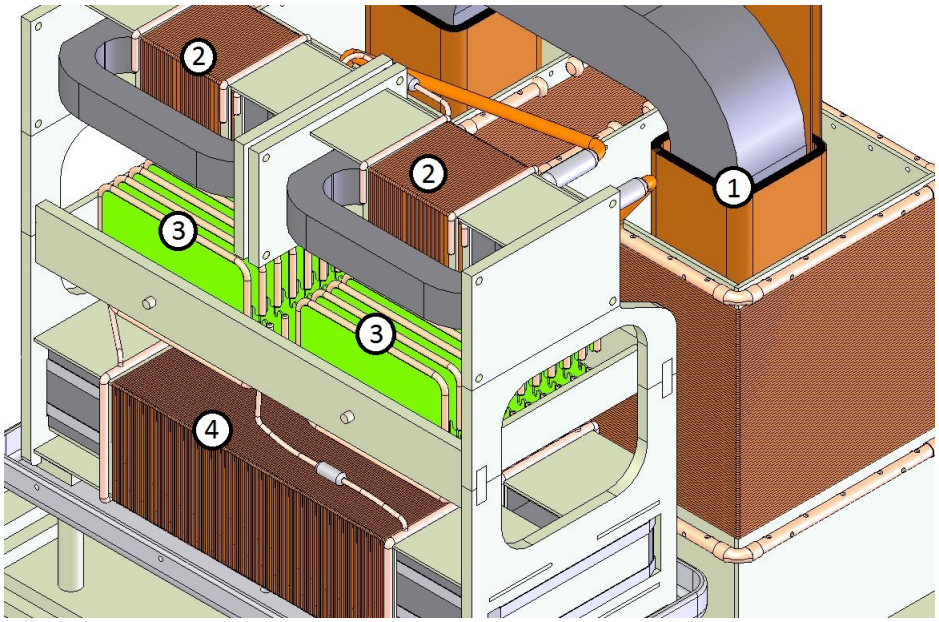

Figure 2: 1) Transformer 2) Common Mode Choke 3) Rectifier 4) Filter Inductor

2.2 Transformer

Figure 3 shows an overview of the complete, assembled HVHF transformer, which is the main object of analysis. The assembly process itself is carried out by a department employee and several important features of this process will be mentioned throughout the report. These mainly relate to the high voltage requirements and will be discussed in subsection 5.2.

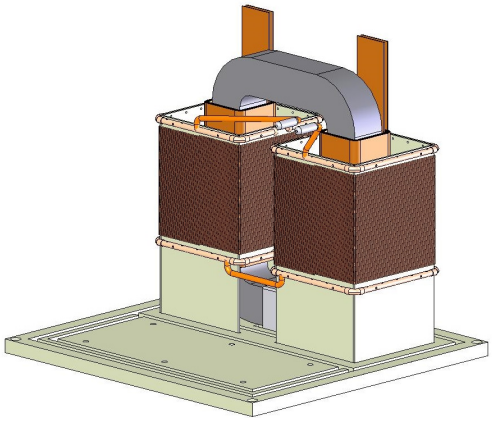

Figure 3: Overview over the transformer. Copper bars with rounded connectors enable connection to the subsystems.

The transformer is of core-type, HVHF adjusted and is constructed with a low loss/high permeability nanocrystaline core. In the following subsections relevant geometrical and physical parameters of the major transformer parts are specified and discussed.

2.2.1 Core

The transformer core used in the project is an uncut and almost rectangular one, apart from the corners which are rounded. Geometric dimensions and shape of the core provided by the manufacturer are shown in Figure 4.

Measurements on the real core sample give following values: core height, 390 mm; outer core width, 290 mm; core depth, 54 mm; core cross section, 57 mm; inner core radius, 20 mm.

The composition of the core is laminated Vitroperm500f strips covered with outer layer of epoxy resin and black paint.

The effective parameters for the core are; area Fe: 22,1 cm^2, length Fe: 103,2 cm, weight Fe: 16.8 kg. The fill factor is 0.7 and lamination thickness is 20 μm.

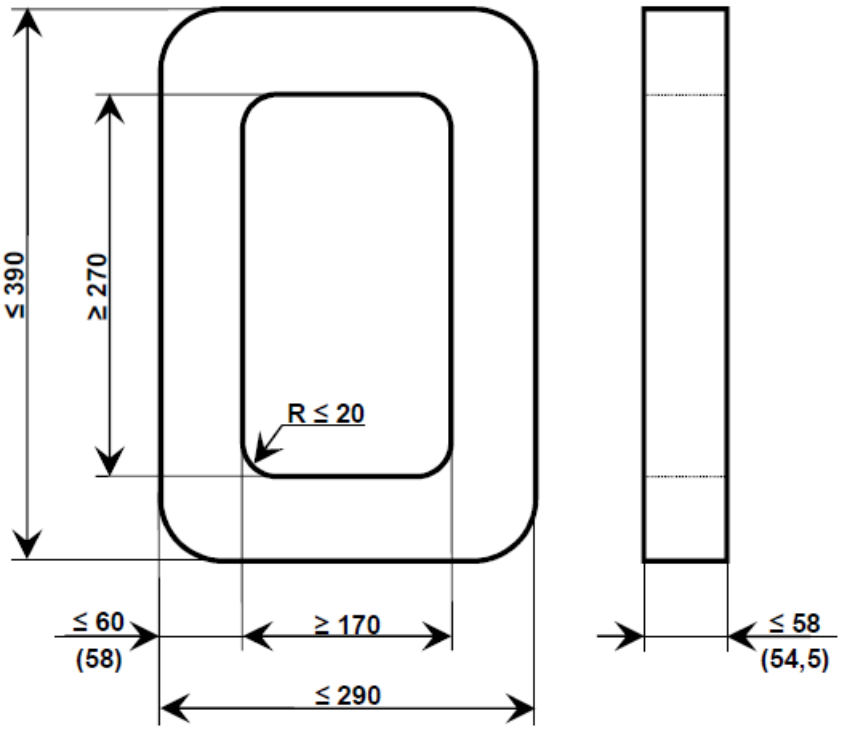

Figure 4: Shape and dimensions of the transformer core [mm]

Furthermore several magnetic and electric properties can be prescribed for the core. These are specific conductivity, relative permittivity and relative permeability. Conductivity of the core parallel to the lamination direction is assumed to be the same as conductivity of Vitroperm500f, namely 0.87 MS/m [6]. While this value is not true for the lamination layers, their conductivity can be considered low enough not to take into account when considering most of the relevant physical phenomena. Relative permittivity typically equals one for metals, however effective value deviates from the starting one with frequency and a number of other parameters [7]. Relative permeability of the core can also be said to be frequency dependent, in addition, this parameter depends on the strength of the magnetic field applied to the material. This results in an highly nonlinear behavior. It is however necessary to take these tendencies into account due to permeability of the core being arguably one of the most important parameters in transformer modeling. This is achieved through construction of a magnetization curve,

frequency dependence is omitted due to high complexity of the phenomena. Throughout the project several magnetization curves were made and used due to the lack of a single one reliable enough. This provided support for construction of several permeability curves. Partially, the curves are built up through local linearization of the relationship between the H-field and B-field according to equation (2.1).

$$\mu_{r\Delta} = \frac{\Delta B}{\mu_0 \Delta H} \tag{2.1}$$

Note that the permeability curves constructed are in fact based on DC magnetization curves. This is an efficient way to represent permeability due to finite element programs often requiring permeability characteristics input of precisely this form.

Below in Figure 5 two permeability curves can be seen. The curve utilized for most of the simulations is designated as "Interpolated manufacturer data". Second permeability curve of plot is based on measurements on the real core.

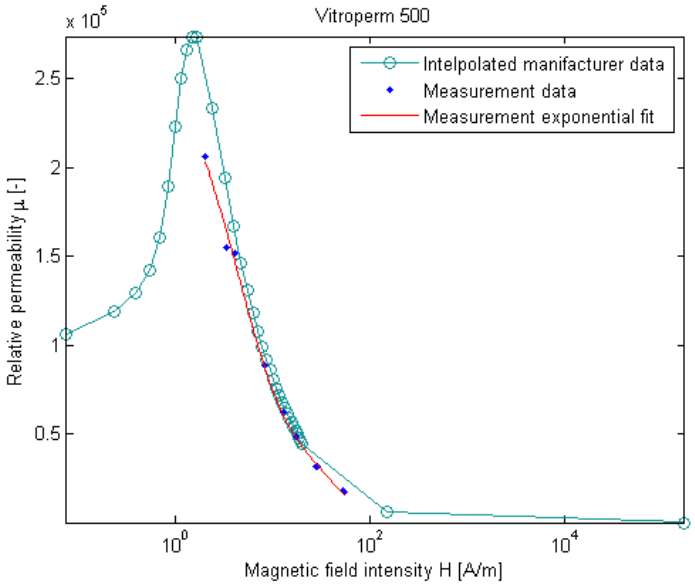

Figure 5: Permeability curves produced from two sets of data; one provided by manifacturer of the core and one acquired through measurements on the transformer

A small number of modifications have also been made to the core throughout the construction process. These consist of two layers of epoxy, specifically bisphenol-A-epoxy and similar adhesives. In between the epoxy layers the core is also covered with electrical tape. These measures were taken due to small particles breaking off the core and contaminating the insulating transformer oil.

2.2.2 Windings

Primary winding consists of two coils with 8 turns each, connected in parallel. Each of the coils are wound around the long sides of the core. The parallel connection is made through a common, horizontal bus coupling which exits each coil on the upper side. Naturally, the coils are wound in different directions resulting in a high total flux Φ_B, when a varying voltage is applied over the parallel bars. The material used for primary windings is copper film with dimensions of 0.003x0.238x2.4156 m. The main physical property, apart from the film's bending qualities, is its conductivity, which is considered to be the same as for copper; 59.6 MS/m [1]. It should be noted that this parameter varies with temperature, which in general could imply design constraints due to Joule heating of the wire. As discussed in 2.2.1 the permittivity of metals is a non-trivial parameter and can be said to equal 1 without introducing significant errors, for the sake of simplicity.

Secondary winding of the transformer is composed of 200 turns of enameled copper wire separated into two windings of 100 turns each which are then connected in series. The conductive diameter of the wire is 1.4 mm and its total length is 126.4 m. While the primary winding can be considered almost circular, secondary winding on other hand has virtually quadratic shape, seen from above.

2.2.3 Insulation & HV components

The transformer and its closest subsystems are placed in a metallic container holding transformer oil which serves both as insulator and coolant. The liquid used is a synthetic, ester - based transformer oil with a permittivity value of 3.2 at 20°C. It is worth to note that a large number of other parameters, less relevant here, exist in association with the oil. Overall the liquid has relatively high fire point and has low environmental impact.

Due to voltage a difference of up to 150 kV between secondary and primary as well as voltage differences between the turns of the windings insula-

tion layers are used in order to prevent flashovers. Anti-corona protection is also implemented in order to prevent high electric fields and to reduce losses.

On the primary side, between the core and the winding a glass fiber insulation layer is made. This enables the winding not to be in contact with the grounded core and has a mechanical function of protecting the relatively fragile nanocrystaline core material. The core is grounded to the steel plate found under the fibreglass of the base plate. Outer glass fiber layer of the base plate has embossed patters between the fastening points of the core and secondary winding support in order to increase the creepage distance.

In between the turns of the primary winding, a layer of insulating sheet provides electric insulation. On the secondary side lamentation of the wire provides the isolation between the turns. The secondary winding is separated from primary by a gap of 40 mm.

Anti-corona rings are mounted along the lower and upper edge of the secondary winding, these are copper tubes with smooth edges and a mean diameter of 10 mm. Round holes are drilled into the tubes in order to enable transformer oil to fill the cavities.

2.2.4 Support Structures

In order to keep the magnetic and conducting parts of the transformer in place, as well as ensure that the creepage and clearance margins are maintained the transformer is mounted on a sturdy support structure.

The core is fastened to the ground plane covered with an outer fiberglass layer. The metal strip holding the core in place is not closed in order to reduce the amount of current induced in it.

Secondary winding is held up by a fiberglass support structure which encircles the core. Fiberglass is the material of choice due to its good compatibility with oil, its low conductivity and its mechanical strength.

A number of sophisticated support structures made of fiberglass are also deployed for nearby subsystems as seen in Figure 2. Main consideration in their design are also creepage and clearance distances.

Relative permittivity of the fiberglass used is 4.5.

2.3 Subsystems

The subsystems, presented in Figure 2 are attached to the main transformer and/or each other using rigid copper pipes. The HV requirements are reduced at this stage in the system due to none of the subsystems having a coupling to the low voltage side of the system. The expected voltage across the components, based on which the anti-corona devices, creepage and flashover distances are dimensioned, is 25 kV.

2.3.1 Common Mode Choke

The common mode attenuating choke is composed of two smaller cores with following dimensions: core height, 170 mm; outer core width, 77 mm; core depth, 24.5 mm; core cross section, 19.4 mm; inner core radius, 17 mm. The core is composed of nanocrystalline material Nanoperm and has a relative permeability of 30 000 before saturation, after which the value is reduced drastically. The specific conductivity of the material is 0.87 MS/m just as for the transformer core. The choke is connected in series with lower and higher voltage side of the secondary winding.

Two windings of 40 turns, 1.4 mm diameter, copper wire each are applied to the long side of each core and then series connected with their respective counterpart on the other one. Both windings rest on fiberglass supports with specially designed access points arranged to provide insulation for 25 kV of voltage difference over the secondary side of the transformer.

2.3.2 Rectifier Bridge

Rectifier bridge is composed of two stacks of 11 Printed Circuit Boards (PCBs) each, connected in series. Each PCB holds power diodes which are in turn connected in series. Along the edges of the PCB runs an anti-corona ring with a distance of 10 mm to closest consecutive PCB. The stack is stabilized and held in place by plastic connector connecting all boards.

Connections from the common mode choke to the rectifier bridge are made by copper pipes and enter the stack at middle point of the respective half.

2.3.3 Filter Inductor

Final subsystem consists of an iron core filter inductor. The core is composed of two separate U-shaped halves made of silicon steel sheets with laminate

between each layer. Permeability of the silicon steel is, similarly to the other materials, nonlinear as a function of magnetic flux density, pre-saturation value can be considered to be 9000. The air gap between the core halves is 5.6 mm. Other geometric parameters of the core halves are: core height: 175 mm, outer core width: 137 mm, core depth: 55 mm, core cross section: 50 mm. Two series connected windings are applied to the long sides of the core, these have 200 turns of 1.4 mm diameter copper wire each.

The filter inductor is connected in series with the higher potential terminal of the rectifier stack. Its output serves as connection point for another 25 kV module which is then coupled in series.

2.4 Requirements

The transformer under analysis must fulfill several criteria, both when it comes to power and current output, reliability under operation and amount of space one unit is allowed to occupy. Because the requirements are not carved in stone, they serve more as guidelines to follow under the course of the project.

2.4.1 Requirements under Operation

It is planned that klystron feeders should have a lifespan of at least 25 years, which sets expectations high on lifespan of an average subsystem. The transformer must therefore be able to stay operational for extensive amounts of time, setting the bar for the degradation qualities of all included materials. This is a though requirement when taking into account HV, HF and high electric and magnetic fields associated with operation at full capacity.

Basic input/output requirement on the isolated prototype transformer is the ability to convert 15 kHz square wave from a voltage of 1 kV to a Voltage of 25 kV in pulses of 3.5 ms. While the excitation voltage will have fast rise and fall times, the output is not required to be as sharp.

A more realistic way to look at requirements might be to take the surrounding subsystems into account. The requirement for a complete unit is an output voltage of 115 kV from six series coupled systems including transformer, common mode choke, rectifier bridge and a filter inductance. This HV pulse should have constant voltage, low ripple and be 3.5 ms long with a rise time of maximum 100 μs. When the problem is considered this way it becomes clear that the main requirement on the transformer is as low voltage difference as possible over the parasitic elements of the design without

jeopardizing the reliability and the HV insulation.

2.4.2 Spatial Requirements

Apart from the requirements on performance of the transformer there are spatial requirements on the size of the system. Main reason for this is that around one hundred klystron modulators will be installed at the ESS facility, each requiring a pulse transformer system. Each of the systems then require six of component chains described in Figure 1. Making the system compact is therefore essential in order to reduce the amount of insulating and cooling oil, which will need to be replaced several times during the operational time of the facility. Naturally requirements on size of the system also come for amount of space currently planned for the RF system and spacing associated with repair and service of the components.

3 Transformer Models

Due to wide use of transformers in power grids on HV and LV levels, in electronics and immense amount of other tools and devices there exists a variety of well defined transformer models. These range from grid based models, focused on load flow, capacity and fault protection to schematic or graphic models which take into account inner functioning and parameters of the transformer. A further separation can also be made between electromagnetic, electrostatic and thermal models.

The models are needed to break down a complex structure to a number of parameters which can be studied separately. The results of the model testing are then used to predict the behavior of the real electrical device.

In single phase HVHF application, as the one being examined in this report, a large amount of models can be found less useful. While three phase models are suitable for grid applications such as transmission and distribution networks, they are unsuitable for a transformer not being a part of the three phase network. It can be noticed that these models seldom take into account HF effects due to 50 Hz/60 Hz sinusoidal nature of a typical power grid. The design evaluation performed requires models that offer a good parameterization of the physical aspects of the transformer. This limits the spectrum of suitable models to ones that take into account features beyond the principal function and somehow include physical aspects of the core, lamination, windings, dielectrics and other components present. It should be noted that many of the models require a large amount of computational power and are best suited for implementation through a computer-based numerical solver. While simpler models can be implemented by hand though, for example, MATLAB scripts, other can utilize existing tools like FEMM or Comsol.

When it comes to the electromagnetic aspect of the transformer, a set of equivalent circuit models exist. These provide basis for the electrical equivalent of the transformer and can include most of the essential electromagnetic physical properties of the device. This model is further discussed below in 3.1.

While fulfilling their purpose as system models for the whole transformer the equivalent circuits themselves need to be provided with input parameters. This data can be acquired either directly from the transformer, if measurements can be performed, or it can be provided via analytic or numerical calculations. Choice of method used for parameter acquisition is widely determined by accuracy required as well as time and instruments available.

3.1 Equivalent Circuit Models

Equivalent circuit models might be among the most common, well studied and useful models for transformer design. In one or another form they are present in most of educational literature as well as a variety of transformer design and analysis studies. Depending on the aspects discussed and the precision desired, the equivalent circuits might include a small or large amount of components. These components can then be distributed in varying manners, depending of level of detail necessary [2] [3].

Careful analysis of the transformer and its parameters requires a model including a representation of vast majority of the equivalent circuit components. Below, in Figure 6, such model can be seen. An explanation for each of the included components is presented in Table 1.

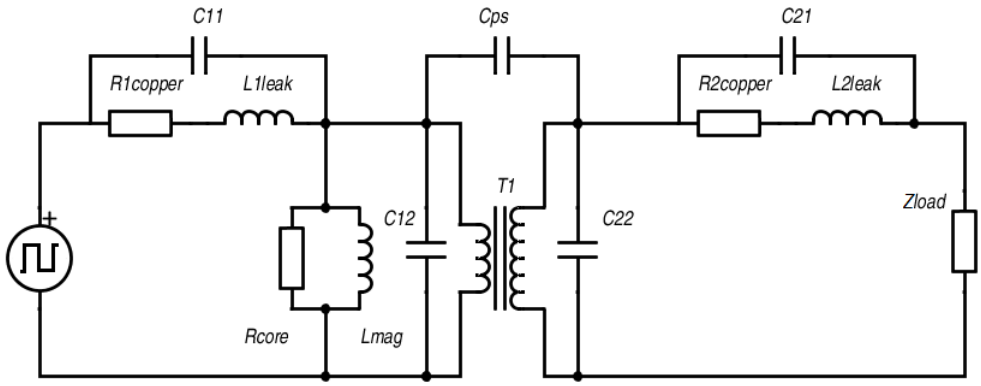

Figure 6: Equivalent circuit model for HF transformers

Depending on the geometry of the transformer, especially the winding arrangement, as well as the frequency range where it is operational, several components will typically be of more importance. In the transformer under consideration, L_{1leak} and L_{2leak}, are of big importance due to high insulation distance between the the primary and secondary winding resulting in considerable flux leakage. Considering the 15kHz pulsed excitation, capacitive effects are typically of much higher importance than in low frequency transformers due to stronger capacitive coupling through parasitic capacitances. This means that C_{12}, and C_{ps} will play a significant role in the behavior of the transformer. Capacitances C_{11} and C_{21} are also present, but are typically of less impact due to most of the capacitance being dis-

R1copper	Resistance of the primary winding
L1leak ($L_{1\sigma}$)	Leakage inductance referred to the primary side of the transformer
C11	Capacitance related to high frequency effects in the primary winding. Typically associated with proximity effect and nonlinear voltage distribution along the winding resistance and leakage inductance.
Rcore	Resistance associated with losses due to hysteresis, proximity and eddy - effects in the transformer core
Lmag	Magnetization inductance closely related to self inductance of the primary winding
C12	Capacitance between the turns of the primary winding.
Cps	Capacitance between primary and secondary winding
T1	A representation of an ideal, lossless transformer
C22	Capacitance between the turns of the secondary winding.
C21	Capacitance related to high frequency effects in the secondary winding. Typically associated with proximity effect and nonlinear voltage distribution along the winding resistance and leakage inductance.
R2copper	Resistance of the secondary winding
L2leak ($L_{2\sigma}$)	Leakage inductance referred to the secondary side of the transformer
Zload	A load connected to the output terminals of the transformer

Table 1: Table of components included in equivalent circuit model [3] [4] [9]

tributed in parallel with L_{mag} and R_{core} in the studied frequency range [4]. C_{22} is of less interest due to secondary winding being composed of large amount of wire turns which can be said to have relatively small capacitive coupling between them in comparison to the primary winding. This is despite secondary capacitance often being of significant size after referring it to primary side.

Several other electrical equivalent circuits choose to merge capacitances C_{11}, C_{21} and C_{12}, C_{22} respectively. The resulting components are then placed in parallel with either the voltage source or the load [3]. It is nontrivial which model that is to be chosen for modeling the transformer. As mentioned, frequency range is a good indicator of how well distributed the

capacitances should be in order to represent reality credibly. For the performed analysis the component distribution is chosen empirically after iterative matching of circuit measurements to simulation with different component configurations. The final model used for circuit simulation is a slight modification of Figure 6, where C_{11} and C_{12} as well as C_{22} are set to zero. The modification is made primarily due to good match with measurement results, further development of the model is however possible using good estimation of the mentioned capacitances.

3.2 Parameter Acquisition

It is clear that the success of modeling a transformer using an equivalent circuit model is highly dependent upon careful selection of the values among the equivalent components. These values are possible to acquire using several methods which differ in accuracy and often depend on the geometric complexity of the transformer.

The three methods presented are: analytic estimation which uses modified or existing mathematical models, measurement based estimation based on lab data and finite element estimation which uses computer based simulation. The advantages and drawbacks of each method are discussed and parameter values acquired using them are presented in sections 3.2.1, 3.2.2 and 3.2.3.

3.2.1 Analytic

Analytic method typically offers a quick estimation of what order of magnitude that can be expected from a transformer parameter. While in some cases offering excellent results, as in estimation of self inductance of a toroidal core or capacitance between two flat parallel surfaces, this method is complicated and perilous in cases when the geometry is considerably more advanced. While it might be possible to analytically model more advanced shapes, it is a daunting task to attain the desired values due to complex integration issues which arise with the geometry.

In case of $R_{1copper}$ and $R_{2copper}$ a good approximation can be made with help of a simple and relatively accurate model for classical linear DC resistance, see equation (3.1). This approximation works well due to constant thickness of copper used for primary and secondary windings, but also because skin and proximity effects do not play a significant role in the analyzed windings with an excitation of 15 kHz square wave.

$$R = \rho \frac{l}{A} \tag{3.1}$$

It is, however, important to estimate the relevance of such effects when modeling the windings. In case of skin effect, a check can be performed using equation (3.2) [1]. Solving the equation for a given angular frequency ω gives the depth into the conductor at which current density J decreases to a value of $\frac{J_0}{e}$. The formula is valid for harmonic waveforms and in order to get a credible result for the square wave a decomposition into a Fourier series can be applied.

$$\delta = \sqrt{\frac{2\rho}{\omega \mu_r \mu_0}} \tag{3.2}$$

After estimation of the skin depth δ a new value of AC resistance is calculated using (3.1). This time with a reduced area equal to the area of a hollow metal pipe with wall thickness of δ. The process is then optionally repeated for higher frequency components of the Fourier decomposition. Important to notice is that resistances calculated this way should not simply be added in series OR in parallel. A more accurate approach is to multiply them by a scaling factor before adding the resistances in series. Estimation of a good scaling factor is outside of scope of this thesis due to skin effect being more or less negligible.

The skin depth for 15 kHz sinusoidal excitation in copper wire of the secondary winding is 0.53 mm, with the radius of the wire being 0.7 mm this results in a overall conductive area reduction of approximately 6%. For next Fourier coefficient of 45 kHz the area reduction is 31% which is significantly higher, but is effectively of much less importance. Therefore for estimation of $R_{1copper}$ the skin effect is of relatively little importance. Same applies to $R_{2copper}$, due to equivalent qualities of the copper conductor and its large cross section area in comparison to the thickness of the conductor. With a width of 0.3 mm the skin depth for both 15 kHz and 45 kHz exceeds the the dimension of conductor meaning that the current density J inside of it is virtually unaffected.

Proximity effect is overall more complex phenomena to analyze analytically, due to the effect being highly dependent on winding arrangement,

conductor shape and magnetic properties of materials in proximity to the winding analyzed. Although some analytic expressions exist for a number of winding arrangements a more clear picture can be attained using computer aided simulations. A further study of proximity effect will be done in section 3.2.4.

Calculation of L_σ is performed in several different ways. Two of the approaches used consider the space between primary and secondary winding, due to highest magnetic leakage fields lying in this precise volume. First proposed method is to consider the energy stored in between the windings and from that derive a value of inductance through (3.3) [5]

$$L_\sigma = \frac{\left((d_{ins,i} + \frac{K}{8})^2 + K^2\right) N_{LV}^2 \mu_0}{16c} \tag{3.3}$$

where $d_{ins,i}$ is the insulation distance between primary and secondary winding, K the perimeter of the primary winding, L_σ the leakage inductance, c height of the primary and secondary winding, which are assumed to be equal, N_{LV} the number of primary turns and μ_0 the vacuum permeability. Note that this approach is only valid for core type transformers with equal height of the windings.

For the design considered in this thesis the result given by (3.3) is unreliable due to different height of the windings on LV and HV side. By adjusting the volume in which the magnetic energy is stored in derivation of the formula, it is however possible to improve the results.

A more straightforward method of evaluating L_σ is to approximate the volume and the windings with a air core solenoid. The self inductance of a solenoid is then given by (3.4) [1].

$$L_\sigma = L = \frac{\mu_0 N_1^2 A}{l} \tag{3.4}$$

where L is self inductance of the solenoid, N_1 is thenumber of winding turns and l is length of the solenoid. In this case L becomes the leakage inductance L_σ referred to the primary, low voltage side, N_1 is number of primary turns and A is area between the primary and secondary. This approximation utilizes the fact that majority of the magnetic leakage flux passes between the primary and secondary winding and this volume can

therefore replace a fictive air core of solenoid. Number of turns is taken from the primary coil if the leakage inductance needs to be referred to primary side or from secondary if leakage inductance of secondary is preferable. Though being a rough estimation, this simple model provides a credible result presented in the end of this section.

Magnetizing inductance L_{mag} can be approximately estimated by applying Ampere's and Faraday's Law on a toroidal core. See equations 3.5 [10], 3.6 [10] and 3.7 [1].

$$\oint_C Hdl \ = I_{enc} \tag{3.5}$$

where $\oint_C$ is the line integral along a closed loop, in this case inside the toroid, H the magnetic field intensity and I_{enc} is the total current encircled by the line integral.

$$E = -\frac{\Delta\Phi_B}{\Delta t} \tag{3.6}$$

where E is induced electromotive force and $\frac{\Delta\Phi_b}{\Delta t}$ the change of the magnetic flux over time.

$$L_{self} = \frac{\int v(t)dt}{i(t)} \approx \frac{\mu_0\mu_r N^2 A}{2\pi r} \tag{3.7}$$

where L_{self} is self inductance of the system, N is number of coil turns, in our case in the primary winding, A is the cross-sectional area of the core and r is the mean radius of the toroid.

It should be noted that this approximation implies uniform magnetic flux density distribution throughout the core, round core shape and tightly wound coil turns. The result can therefore be expected to be slightly higher than in reality unless a compensation is made. Due to core not having a round shape a fictive radius must also be introduced. Based on a effective magnetic path length of 103.2 cm a radius of around 16.4 cm can be used as a substitution.

Also, leakage inductance L_{sigma} is always included into the calculated value of L_{self}. This can either be neglected due L_σ being several orders of

magnitude smaller or adjusted by simply subtracting it from L_{self} as seen in (3.8).

$$L_{mag} = L_{self} - L_{\sigma} \tag{3.8}$$

As presented in 2.2.1 the relative permeability of the core is not constant, meaning that in order to acquire a result close to reality the nonlinear character of this core parameter must be taken into account. Most efficient and accurate way of doing this is computer aided calculation or a direct measurement as will be discussed further in sections 3.2.2 and 3.2.3.

Core resistance, R_{core} is a somewhat more challenging parameter to estimate by analytic calculation. One approach is to consider hysteresis and eddy losses for a certain harmonic frequency and magnetic flux density, in order to then calculate the resistance of the block using corresponding voltage or current. Expression for the sum of the losses can be seen in equation (3.9) [8].

$$P_{tot} = P_{hyst} + P_{eddy} = \frac{mf\hat{B}^2}{\rho 2\sqrt{2}\mu_0\mu_r} + \frac{m\sigma b^2\omega^2\hat{B}^2}{6\rho} \tag{3.9}$$

where $\hat{B}$ is the peak value of the magnetic flux density, ρ the density och the core material, b is half of the thickness of the metallic sheet in the core, and σ the conductivity of the sheet. $\hat{B}$ is in turn acquired through equation (3.6) using a chosen voltage $\hat{U}$. A working point on the permeability curve is also selected in correspondence with the chosen applied voltage.

The resistance value is then acquired in accordance with equation (3.10) [1]

$$P = RI^2 = \frac{U^2}{R} \tag{3.10}$$

It is however often challenging to acquire the material data needed for estimation of this parameter analytically, a more accurate way of estimating this parameter is measurement based methods discussed further in next section.

C_{ps} and C_{12} capacitances can due to geometry of the windings relatively accurately be modeled with help of parallel plate model. The capacitance is then given by equation (3.11) [1]. For C_{ps} the approximation can seem somewhat perilous due to different area of the capacitance plates of outer primary turn and the secondary windings. This can however be adjusted by using a slightly smaller value of A. For C_{12} plate model provides an excellent approximation but must be calculated separately, seven times, for capacitance between each turn of the winding. After the acquisition of each distributed value the resulting capacitance is calculated by adding the total capacitance for each turn in series. An idea of why this provides a credible value if presented in Figure 7, note, however, that the connection is not analytically purely series connection.

$$C = \frac{\epsilon A}{d} \tag{3.11}$$

where ϵ is the permittivity of the medium separating the plates of the capacitor, A the area of the capacitor plates and d the distance between them.

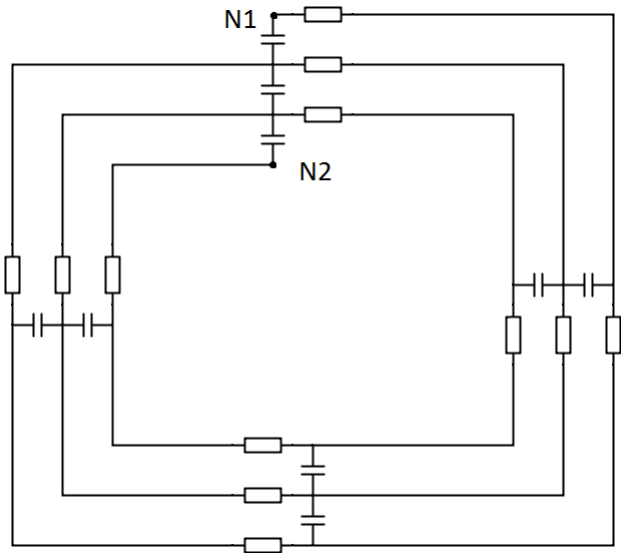

Figure 7: First three turns of the primary winding with distributed series impedance and capacitances

C_{22} On other hand, can not be modeled analytically with the same ease. Closest suitable model is one of two parallel wires, the model is then applied to each side of the secondary winding and thereafter the the resulting capacitances are added in series for each turn of the winding. While only roughly estimated, the capacitance of the secondary wire winding is small and does not contribute significantly to transient behavior of the transformer.

Below, in Table 2, analytically calculated values of equivalent circuit components from circuit in Figure 6 are presented.

R1copper	0.24 mΩ
L1leak ($L_{1\sigma}$)	4.6 μH using 3.4. 1.6 μH using 3.3.
C11	Neglected due to insignificantly small value. Modeled as open circuit.
Rcore	1113 Ω at $\mu_r \approx 200000$ with corresponding $\hat{B}$.
Lmag	33 mH at $\mu_r = 200000$
C12	0.36 nF in air.
Cps	19.6 pF using 3.11 with $A = A_1 = A_2$, in air.
C22	Neglected. Rough estimation in air gives 0.05-0.1 nF when referred to primary. Modeled as open circuit.
C21	Neglected due to insignificantly small value. Modeled as open circuit.
R2copper	1.44 Ω
L2leak ($L_{2\sigma}$)	2.9 mH

Table 2: Analytically calculated equivalent circuit parameters

Apart from parameters directly used in the equivalent circuit, conductivity of the core is estimated using equation (3.12) [8]. The performed calculation provided a reference value to compare to the conductivity presented by the manufacturer.

$$\sigma = \frac{6\rho p_e}{b^2\omega^2\hat{B}^2} \tag{3.12}$$

where p_e is eddy power losses, b is half of the thickness of the metallic sheet in the core and ρ is density of the core material. Value estimated using the formula is 0.28 MS/m while the value read from the datasheet is 0.87 MS/m. Both values were used during analytic estimation and finite element simulations in order to refine the equivalent circuit parameters.

3.2.2 Measurement Based

Measurement based estimation of parameter has a significant advantage compared to analytic and simulation based ones. Every magnetic core typically has smaller or bigger defects and with high probability deviates from the datasheets if such are provided. In case of the current project and the specific core under analysis this is very relevant. Due to the material being relatively new and the core not being mass produced, well documented product, many parameters associated with it are either unreliable or missing. This results in difficulties and inaccuracy when using either of the other equivalent circuit parameter acquisition methods. Using data from measurements, on the other hand, takes into account the flaws of the sample core and can therefore provide a large amount of accurate information assuming good instruments and correct procedure.

The weak side of the method is the necessity of being able to make measurements on the transformer. This is not always an easy task due to transformer often being placed in oil tank, and in current project being under continuous construction. Apart from this, a test setup is also needed. While some tests do not require large amounts of equipment, other, especially related to HV and HF, need a number of specific apparatus. Unavoidably the quality and precision of the measurement equipment will also play a role in the accuracy of the results.

In the list below useful testing equipment is listed.

Oscilloscope
: For waveform measurements, transient analysis and overall data collection. If transformer parameters are to be deduced from voltage and current waveforms data needs to be able to be exported for analysis.

Current measurement and HV probes
: In order to make measurements on high currents and voltages specific probes are required. For current measurement current clamps can be employed. For high voltage a wide selection of specialized probes are available.

Power Source
: Power source is a crucial piece of equipment in transformer testing due to nonlinear behavior of the transformer. Optimally the source should be able to feed a heavily loaded transformer in a broad frequency range

with both sinusoidal and non sinusoidal waveforms. This is necessary in order to analyze the pulse response and saturation behavior at different working points.

Dummy load

While working with high currents and voltages a test load able to handle heat dissipation and high voltage is needed.

A variable load can be an efficient way to easily iterate through a range of working points. Depending on the project the load might also need to have inductive or capacitive character. In klystron application the load is modeled as pure resistance with a constant value.

RCL meter

For easy and relatively accurate measurement of capacitance a RCL meter is employed. While frequency dependent resistance and inductive parameters of the transformer can be measured as well, they represent no-load values and do not include the saturation behavior.

Spectrum analyzer

Spectrum analyzer can be compared to a precise RCL meter with a wide frequency band. While also suffering from inability to analyze the flux density dependent saturation characteristics it is excellent for understanding the frequency dependent tendencies of the system.

Data collection for analysis is partially performed using a step down transformer connected directly to 50 Hz electrical grid. While this limits the possibilities to analyze transient phenomena and does not give a full picture of the effects of a 15 kHz square wave, it is sufficient to provide parameters for the equivalent circuit. Further analysis of such phenomena is performed using system simulation and results gathered by other research groups.

A positive side effect of gathering data from harmonic, sinusoidal excitation is the ability to use $j\omega$ method for easy impedance calculation as well as phase angle calculations.

Spectrum analysis is also performed primarily through simulation, even though results from RCL-meter provided an idea of resonance behavior.

A good starting point for transformer testing and equivalent parameter acquisition is conducting the short-circuit test and the no-load test. Short-circuit test is conducted by short-circuiting the primary or secondary winding and applying voltage to terminals of the other winding while measuring the resulting current and power. From these values the series parameters of

the equivalent circuit are calculated with ease through Ohm's law and its implications, seen in equation (3.13) and (3.10)

$$U = RI \Rightarrow V = ZI \tag{3.13}$$

To determine $L_{1\sigma}$, $L_{2\sigma}$, $R_1 copper$ and $R_1 copper$ the values are deduced from total, complex impedance either through measurement of real power P or through phase angle difference θ according to equation (3.14).

$$\theta = tan^{-1}\Big(\frac{\omega L}{R}\Big) \tag{3.14}$$

No-load test is conducted by leaving one of the windings open while applying voltage over the terminals of the other one. In order to keep the test voltage low it is suitable to apply rated voltage to the low voltage side of the transformer. Through this test the parallel parameters of the equivalent circuit are acquired. R_{core} is deduced through the power measurement, which as in short-circuit test presents virtually only real power, P, then with known applied voltage the value is calculated through (3.13) and (3.10). The inductance L_{mag} is then calculated by calculating the current through the other parallel branch. An alternative way to calculate the parameters is through the phase angle, if it is available from, for example, oscilloscope measurement. In that case equations (3.15) and (3.16) can be used.

$$L = \sqrt{\frac{|Z|^2}{\frac{\omega^2 tan^2(\theta)(tan^2(\theta)+1)}{tan^4(\theta)+2tan(\theta)+1}}} \tag{3.15}$$

$$\theta = tan^{-1}\Big(\frac{R}{\omega L}\Big) \tag{3.16}$$

If the calculation of the parameters is based on the real power measurements it is necessary to ensure that the used values do not have a significant reactive power component. It is also worth to note that parameters obtained

will be referred to the side where the test voltage is applied.

Capacitances C_{ps} and C_{12} are estimated through RCL-meter measurements between primary and secondary and over the primary winding respectively. R-C mode of the RCL-meter is used in both measurements. Due to resonant nature of LC-circuits it is advisable to measure the parameters in a broad frequency range in order to detect and understand unexpected behavior.

Apart from the values immediately used in equivalent circuit model, saturation behavior is also possible to extract from measurement data if current and voltage waveforms are available. This is done by numerical integration of the applied voltage according to (3.6) in order to acquire B and (3.5) in order to acquire H, plotting these against each other for one period results in a hysteresis loop. In Figure 8 a typical sample waveform is displayed.

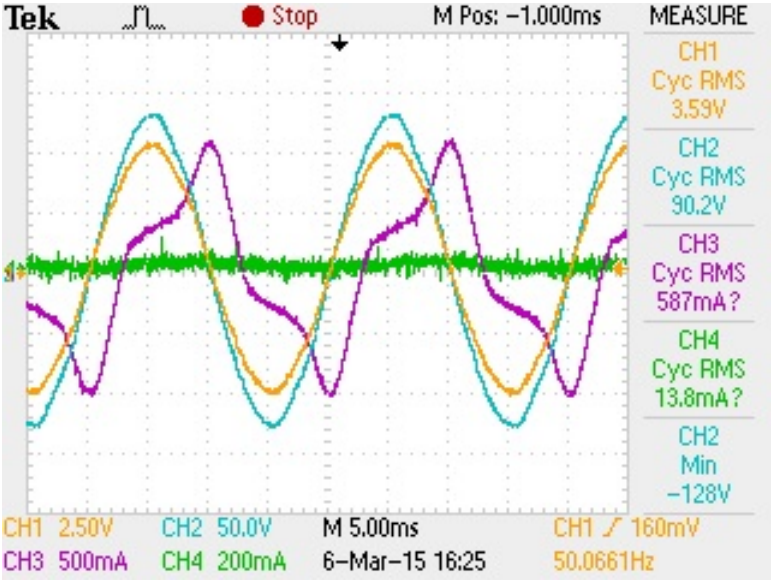

Figure 8: Open circuit sample waveform with mild saturation starting to become apparent

By iterative plotting of hysteresis loops for different input voltages and saturation levels it is possible to not only estimate the hysteresis loss per cycle at different magnetizations, but also construct a permeability curve. A number of measured, calculated and plotted hysteresis loops can be seen in Figure 9.

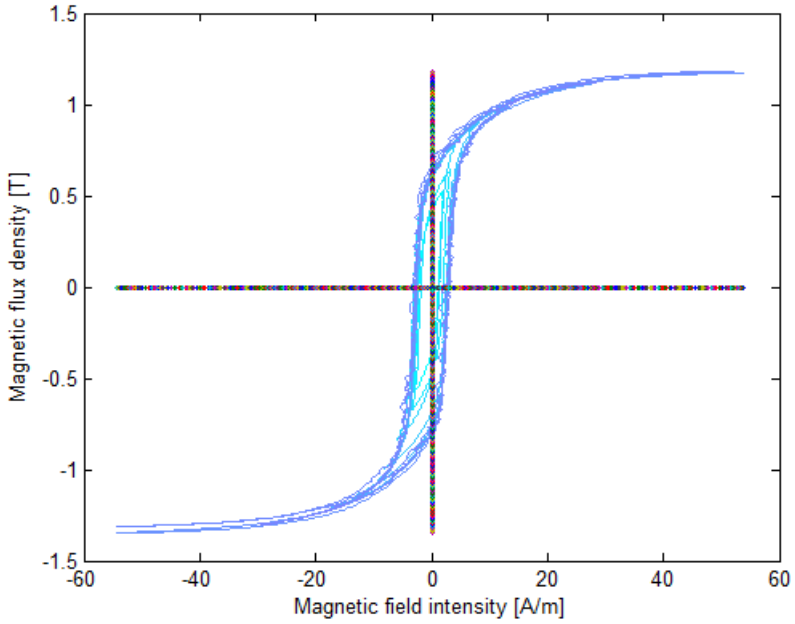

Figure 9: Several hysteresis loops for different magnetization levels

Hysteresis loss, P_{hyst}, is estimated by integration of the area encircled by the hysteresis loop. Because the the data is based on a excitation voltage with a frequency of 50 Hz, virtually no eddy or anomalous losses are included in the loop area. When the loss per period is estimated it can then theoretically be extrapolated for any harmonic wave with a given frequency without loss of accuracy. Total hysteresis loss for the core at 15 kHz is plotted in Figure 10. This provides an idea of how large the hysteresis loss is for a 15 kHz square wave. Notably hysteresis loss increases with magnetic flux density at a ratio proportional to $\hat{B}^{\alpha}$ where α depends on the shape of hysteresis loop and is usually $1.5 < \alpha < 2.6$. For the core under analysis $\alpha \approx 2$. This parameter gets increasingly more important with the operation frequency of the transformer, due to more hysteresis cycles being performed per second. However at higher frequencies, for the same core a lower magnetization point is reached, as suggested by (3.6) and the permeability curve in Figure 5. In general, for higher frequencies, eddy losses become dominant due to ω^2 factor in equation (3.9).

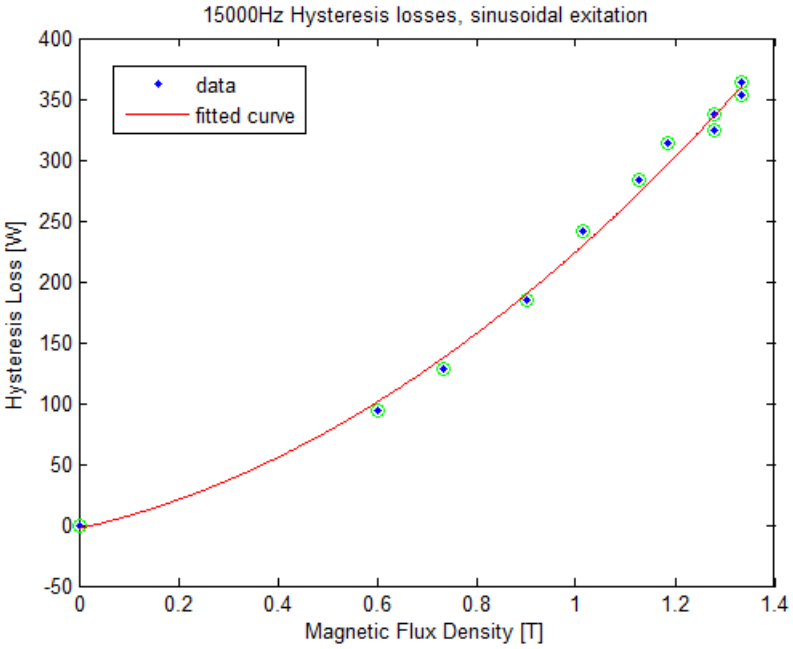

Figure 10: Hysteresis loss extrapolated to 15 kHz and plotted as a function of magnetic flux density.

Relative permeability of the core is acquired from the positive maximum values of each hysteresis loop and is calculated through (3.17).

$$B = \mu_0 \mu_r H \tag{3.17}$$

Optimally the core should not be in use before the first, virgin curve is measured and constructed due to the magnetic remanence of the core material. This means that after the core has been conducting magnetic flux, especially close to or in the saturation region, its magnetic properties are slightly changed. This effect does usually not cause problems under operation but can somewhat distort measurements, as can be expected in the measurements made.

The relative permeability acquired this way can be seen in Figure 11. Same curve can be seen plotted with a logarithmic x-axis in Figure 5, ac-

companied with permeability curve constructed from values provided by the manufacturer.

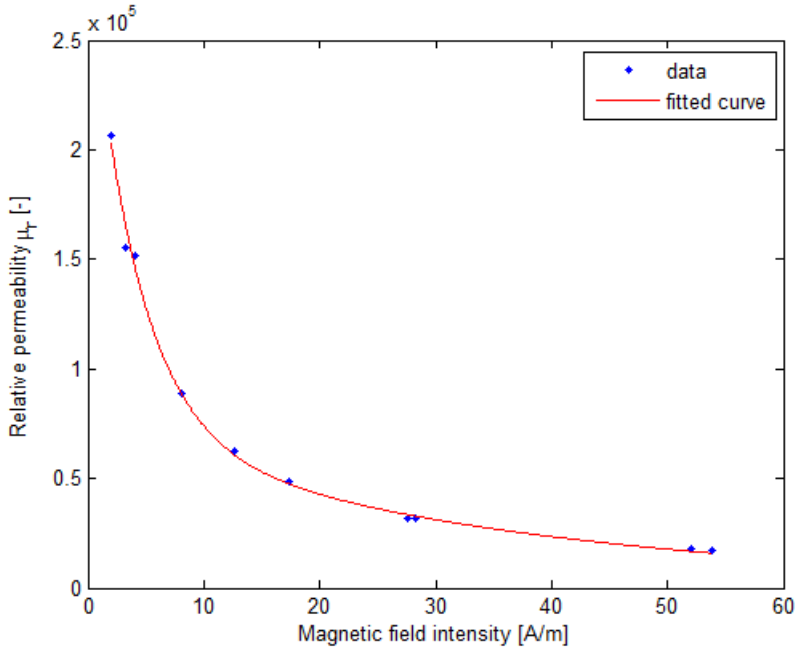

Figure 11: Permeability of the transformer core as a function of magnetic field intensity, based of waveforms from 50 Hz open-circuit test

Equivalent circuit parameters acquired from measurements are unlike those calculated with simple analytic models not linear. This is explained by the fact that values that are assumed to be constant in analytic models are in fact variable or that dependency on a parameter exceeds or is below the expectation. L_{mag} and R_{core} are dependent on $\hat{B}$ due to saturation behavior. The two above mentioned parameters as well as R_{copper} are also frequency dependent beyond the standard models. In case of R_{core} the effect is due to anomalous losses which are not included in the analytic model while for R_{copper} the dependency is mainly caused by skin and proximity effects. Anomalous losses occur due to Barkhausen jumps, which result in local eddy currents in the core [12]. These are safe to neglect in measurements at 50 Hz, lack of these losses can be seen in the shape of the hysteresis loop. For higher frequencies, however, they can be considered as they are

proportional to $f^{1.5}$ [13]. The frequency dependence of L_{mag} is primarily due to a delay between H and B fields in the core, this phenomena results in change of imaginary part of the magnetic permeability which is significant at high frequencies. Primarily this affects the value of R_{core} [14].

In the Figure 12 the L_{mag} is seen, plotted as a function of the magnetizing branch current.

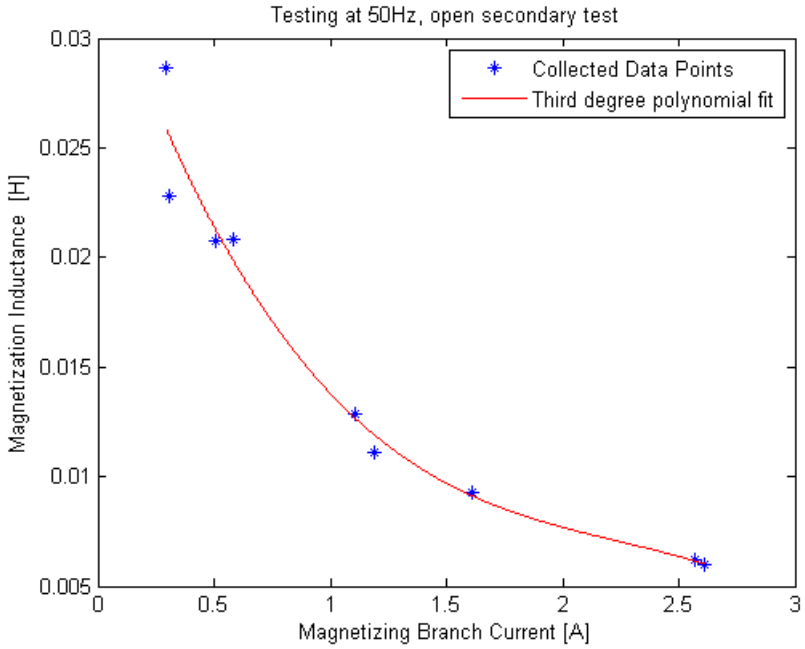

Figure 12: Magnetizing Inductance acquired through measurements at 50 Hz

In reality the magnetizing inductance does only locally have a polynomial - like shape, outside of the plotted region one can expect different behavior. This is primarily due to lower permeability values at low magnetization levels. This behavior is visible in finite element simulation performed in 3.2.4.

Another measurement of L_{mag} is made using the LCR - meter, however instead of sweeping through different magnetization levels the varied parameter is frequency. The unmanipulated data is plotted in Figure 13. It is clear in the figure that the measured value is not constant and has an resonant peak at around 10 kHz. The instrument also returns negative values

past the peak, which are problematic to interpret due to lacking information about the device. Through comparison to typical frequency characteristics of other inductive components assumption is made that the negative values can in fact be understood as normal, positive ones.

Notably, the LCR - meter applies a voltage of 1 V during the sweep, which means that the measurements done are at a low magnetization level.

The 10 kHz peak seen in the Figure 13 does appear in several measurements performed with same LCR - meter. Due to the peak being located relatively low in the frequency spectra self - resonance of single component can be precluded. However the nature of the resonance strongly resembles resonance in a more complex LC or LCR circuit, which the transformer happens to be in accordance with the equivalent circuit model.

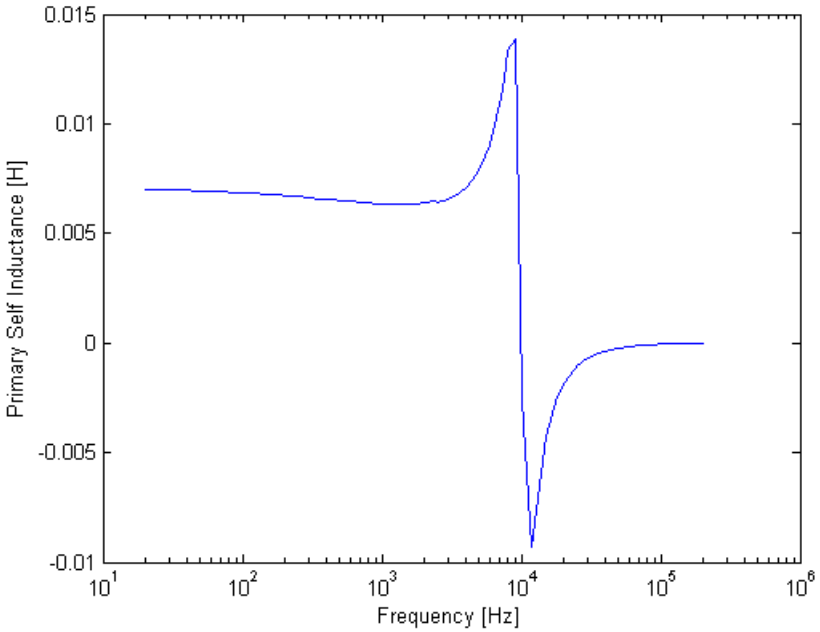

Figure 13: Magnetizing Inductance acquired through measurements with LCR - meter

Several sanity checks were done using simple, hand-held LCR-meters conducted at available frequencies, resulting in values presented in Table 3. As can be seen, the values agree relatively well with the ones read from Figure 13.

Interestingly, neither of the latter two measurement provides a clear value of L_{mag} at the frequency of 15 kHz. Naturally an apparent value can be read from the graph in Figure 13, but it remains unclear if parameter values at resonance frequency can be proven to be a valid estimation of the effective value.

Instrument	AC Frequency	Inductance Value
Numbr. 1	120 Hz	6.65 mH
Numbr. 1	1k Hz	6.62 mH
Numbr. 2	120 Hz	6.67 mH
Numbr. 2	1k Hz	6.61 mH
Numbr. 3	10 Hz	6.51 mH
Numbr. 3	120 Hz	6.71 mH
Numbr. 3	1 kHz	6.65 mH

Table 3: Magnetizing inductance L_{mag} measured using several simple, hand-held LCR-meters

Leakage inductance, L_σ is similarly estimated both through the short-circuit test at 50 Hz at different magnetization levels, and through LCR-meter measurement. The results obtained through oscilloscope waveforms and (3.14) gave two reliable values, rest of the data had to be discarded due to difficulty of finding the phase angle θ in poorly resolved oscilloscope output. The two values obtained from 50 Hz measurements are 8.22 μH at 0.6 V and 6.53 μH at 1 V. LCR-measurements are presented in Figure 14. It is apparent that the leakage inductance is slightly larger at low frequencies, which agrees with the numbers received through 50 Hz measurements.

The referred curve in the figure has slightly higher values than the one measured from the primary side. This is despite transformer ratio of 25 being used to refer the values to primary side. Real transformer ratio $\frac{V_{out}}{V_{in}}$ is found to be close to 24 at 1 kΩ load.

An explanation for the curves not being aligned is the measurement procedure itself. The length of the cable when measuring on secondary winding is longer than for the primary measurement. This adds unwanted inductance which is magnetically very poorly coupled to the primary side, resulting in what is interpreted as excessive leakage inductance.

The effect could also be caused by secondary winding having more flux leakage paths available geometrically. While largest portion of the leakage flux passes between primary and secondary it is possible that leakage occurs

in between consecutive turns and on the outside of the secondary winding.

For precision measurements it is advisable to keep the cable length short in order to avoid introducing unwanted parasitic capacitance and inductance.

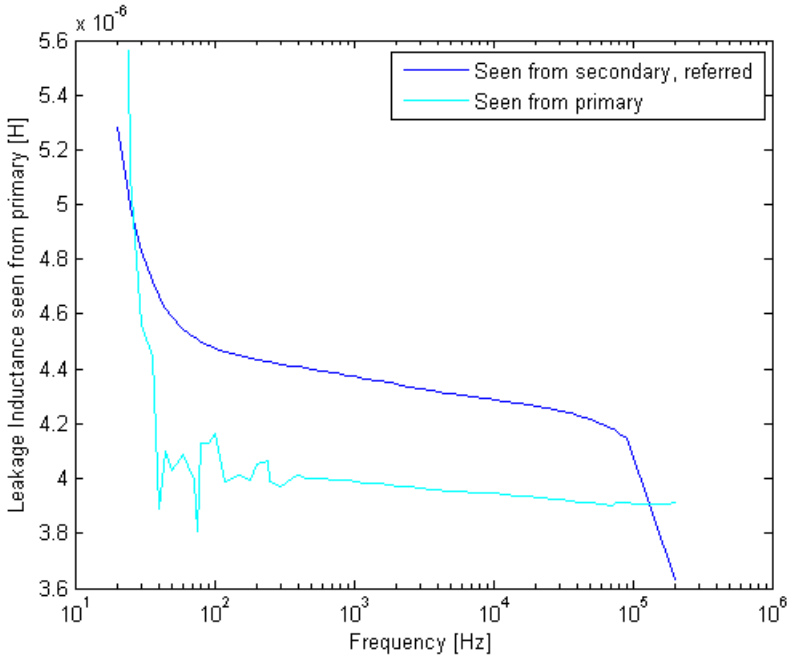

Figure 14: Leakage inductance measured by LCR-meter, the two curves show the values obtained from shorting out primary and secondary, respectively.

$R_{1copper}$ is similarly calculated through phase angle difference at 50 Hz. The same two voltage points of 0.6 V and 1 V, as for L_σ above give values of 0.012 Ω and 0.011 Ω respectively. These resistance values are higher than those analytically calculated which is explained by the voltage and current measurements being performed on the cables leading up to the primary winding instead of the winding ends themselves.

Furthermore $R_{2copper}$ is also estimated based on the oscilloscope data with a result of around 7 Ω. As this result is significantly higher than that estimated analytically, it can be compared to DC measurements done with three independent multimeters: 7.8 Ω, 2.8 Ω and 1.6 Ω. A consensus is therefore not reached. It is expected that the real DC resistance value is close to the analytic result due to good match with the mathematical model. It can

be noted that conventional multimeters have poor precision at low resistance values.

In case of R_{core} a realistic estimation could not be produced using the 50 Hz measurement data. This resistance parameter is closely associated with hysteresis, eddy and anomalous losses in the core, of which only hysteresis losses could be obtained. For an accurate estimation of R_{core}, ideally, real power needs to be measured with an excitation of 15 kHz, 1 kV square wave.

The two essential capacitances, C_{12} and C_{ps} were measured using LCR-meter. R-C mode is used continuously during these measurements. C_{12} is also indirectly calculated during HV insulation test where the capacitive leakage coupling between the core and outer widing is measured. This gives a value of 0.25 pF at 50 Hz in air.

The results from LCR-meter are presented below in figures 15a and 15b.

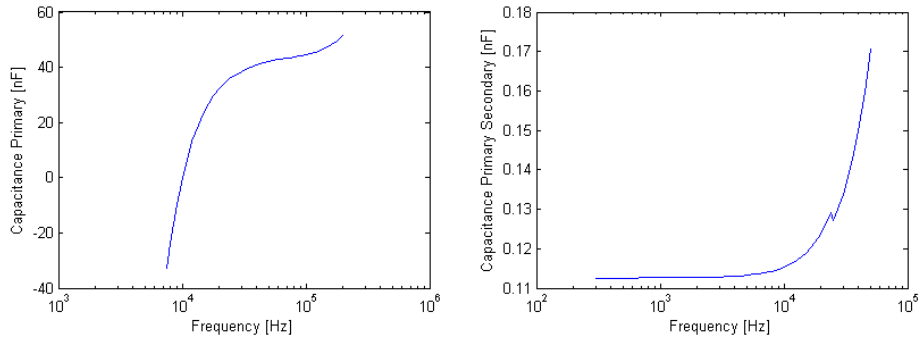

(a) C_{12} *(b)* C_{ps}

Figure 15: Capacitance values plotted as a function of frequency, measured in transformer oil

Unexpected tendencies can be noted in both figures, especially 15a. When compared to Figure 13 it becomes apparent that resonant behavior is visible at around 10 kHz. The capcitance values for primary winding are measured to be orders of magnitude higher than expected. Another control measurement using similar instrument results in capacitance tendencies analogous to those in 15a, see Table 4. These results are further examined in comparison with others acquired through different methods.

Frequency	Capacitance
1 kHz	-3.6 μF
10 kHz	-34 nF
15 kHz	-12.7 nF
100 kHz	6.87 nF
200 kHz	7.48 nF

Table 4: Capacitance C_{12} measured using LCR-meter in air

3.2.3 Finite Element Analysis

Final method of equivalent circuit parameter acquisition discussed in this writing is finite element analysis. This computer aided approach relies on finite element method.

Finite element method is bases on local solution of relevant differential equations. Instead of solving the equations over a complicated 2D or 3D geometry the algorithm breaks down the object under analysis into finite number of small domains with shape of a simple geometrical figure. It is then feasible to through approximation find the potential values at the edges of the geometric shape. A large linear algebraic problem for a wider region is then formed and solved under the condition of minimizing the error between the real differential equation and the approximate one written in terms of other functions. In practice a wide variety of methods for meshing and solving the the resulting problem exist. Solving the problem by hand is disastrously time consuming after applying a mesh, the method is therefore primarily designed to be implemented on computers. The finite element analysis is therefore performed using Finite Element Method Magnetics (FEMM) and COMSOL.

Among the advantages of the method is the ability to model and simulate complex geometries in 2D or 3D without having a real sample available. Another advantage is the ability to visually interpret the results of the simulation due to graphical plots. B-field, H-field, E-field, J - the current density and a variety of other physical phenomena is presented graphically.

An obstacle often encountered while using the method is the difficulty of specifying the model with satisfactory accuracy. Primary issue is lack of reliable material specification, in order to get a life-like, accurate result, most physical parameters must be available for the modeled unit. Another limitation is computational power available, which sets the ceiling for the maximal level of detail in the specified geometry. An associated limitation

is that some geometries require to be modeled in 3D in order to provide credible results, which requires more computational power and time.

3.2.4 FEMM

Finite Element Method Magnetics is a program containing interactive graphical interface and is designed to perform two-dimensional physical simulations. While a variety of physical phenomena can be simulated, the program is used for magnetics and electrostatics. For time invariant magnetic problems FEMM fulfills following equations in the solution region;

(Ampres Circuital Law)

$$\nabla \times H = J \tag{3.18}$$

(Gauss's Law For Magnetism)

$$\nabla \cdot B = 0 \tag{3.19}$$

$$\mu = \frac{B}{H(B)} \tag{3.20}$$

$$B = \nabla \cdot A \tag{3.21}$$

where A is magnetic vector potential. With addition of time harmonics two further equations are added;

$$J = \sigma E \tag{3.22}$$

(Maxwell - Faraday equation)

$$\nabla \times E = -\frac{\partial B}{\partial t} \tag{3.23}$$

Simply put, the program enforces the physical model provided by Maxwell's equations. While understanding of the equations is important for the overview of the physics involved, the program handles all the necessary calculations.

Important to note is that to electrical circuits modeled in the program AC or DC current can be assigned. However no option exists for other types of excitation. Due to this, acquired parameters and other data produced by the simulation bases itself on 15 kHz sinusoidal excitation.

The geometries simulated on are specified in MATLAB, together with material parameters, boundary conditions and other needed input values such as excitation current and frequency. This enables iterative simulation where one or more parameters are automatically changed with each iteration. Selected results of each consecutive simulation are saved to file and are imported to MATLAB for plotting and analysis.

In Figure 16 the magnetic model of the transformer core can be seen.

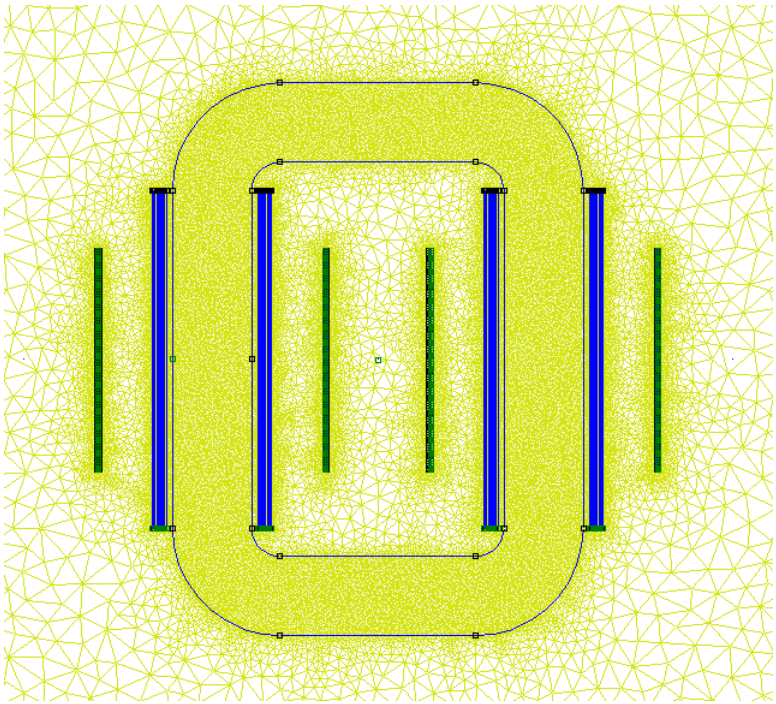

Figure 16: Meshed 2D transformer drawing in FEMM

As FEMM is a 2D program a choice must be made concerning what slice, or surface is suitable for modeling. A depth parameter can then be specified, which in the case of the core provides a precise model. This means that the windings follow the inner and outer bound of the transformer but not the remaining two sides. While this is meaningful for the magnitude of the leakage flux it is in general case satisfactory approximation, among other according to equation (3.5). While the winding turns in the model do not have a visible connection same current is associated with all windings in same group. This means that the each of the parallel primary windings and the all the secondary turns have a group associated with them. In figures 17a and 17b closeup of the transformer windings is seen.

The difference in triangle mesh size across the analyzed region stems from varying need of detail level in different regions. While surrounding air or oil are not expected to exhibit relevant magnetic behavior and therefore have sparse mesh, core and windings instead are densely meshed.

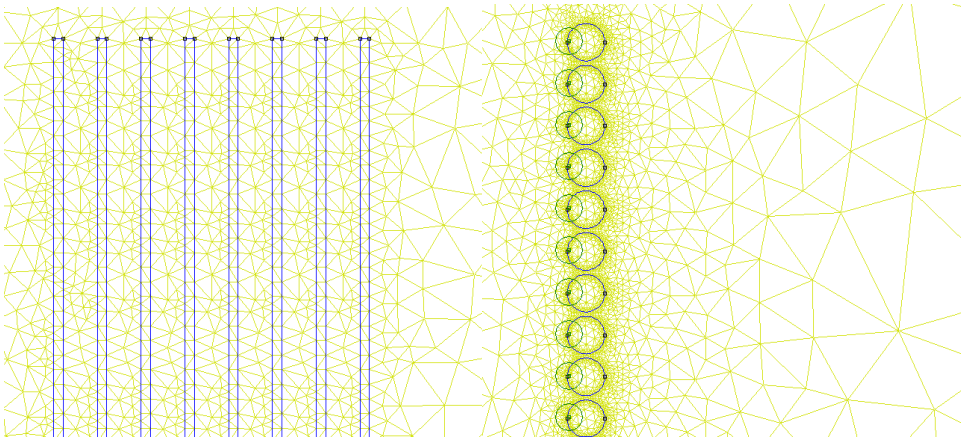

(a) Closeup of the primary winding *(b) Closeup of the secondary winding*

Figure 17: Meshed transformer windings in FEMM. 17a and 17b do not share scale

Parameter acquisition from simulation results is carried out in several different ways. FEMM offers possibility to integrate along lines or contours, as well as over regions and does also present some essential values as default output.

Primary and secondary resistances, $R_{1copper}$ and $R_{2copper}$ are estimated by calculating integral of the total losses over the winding regions and calculating values through (3.10). The values obtained are $R_{1copper} = 0.33m\,\Omega$ and $R_{2copper} = 1.1553\,\Omega$. Because the simulation is carried out at a constant

frequency of 15 kHz the resistance of the windings can be considered to be more of less constant as a function of applied current.

The self inductance, L_{self} of each separate modeled circuit is presented as one of the default outputs. It can however be verified by one or more of following expressions using integral function of FEMM;

$$L_{self} = \frac{\int A \cdot JdV}{i^2} \tag{3.24}$$

where $\int A \cdot JdV$ is integrated over the primary winding cross sections.

$$L_{mag} = \frac{2E}{i^2} \tag{3.25}$$

where E is the energy stored in the magnetic field integrated over the core.

$$L_{mag} = \frac{N\Phi_B}{i^2} \tag{3.26}$$

where the total magnetic flux Φ_B is deduced from line integral of B across core cross section.

The integration is performed with open secondary winding, corresponding to the no-load measurement test. The FEMM simulation integrated upon at magnetizing branch current of 1 A is shown in Figure 18.

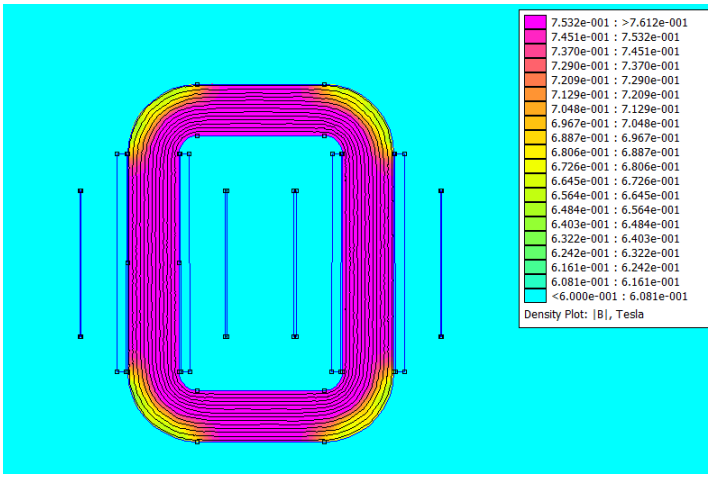

Figure 18: Open circuit FEMM simulation

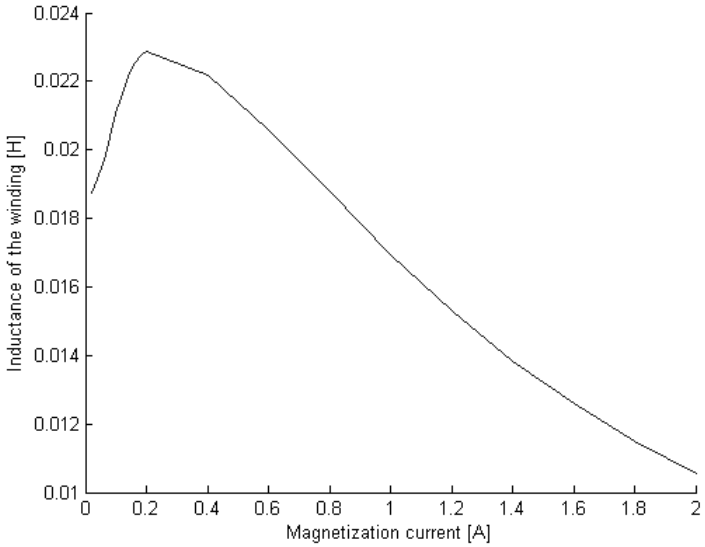

Figure 19: Magnetization inductance as a function of magnetizing branch current

In practice, despite each method making some minor assumptions and doing slight approximation the results from all methods often agree up to 4th decimal. As mentioned earlier L_{self} and L_{mag} follow the simple relationship (3.8). In Figure 19 a plot of L_{mag} is presented, acquired through FEMM simulation.

As expected, a drop in inductance occurs when the core approaches saturation. This happens due to decline of relative permeability which is a factor in self inductance of the winding.

R_{core} can in turn be deduced from the imaginary part of the B line integral over the cross section of the core. This is done using a slight modification of equation (3.26), the fact that harmonic excitation is used and that the R_{core} is frequency dependent. The acquired inductance is multiplied by a factor of $2\pi f$ thereby resulting in an impedance value equivalent to the sought resistance.

Naturally, through modeling R_{core} this way it becomes permeability dependent, just as in case of L_{mag}. This behavior is however expected due to higher core losses being anticipated at higher magnetization levels.

In Figure 20 the equivalent core resistance can be seen.

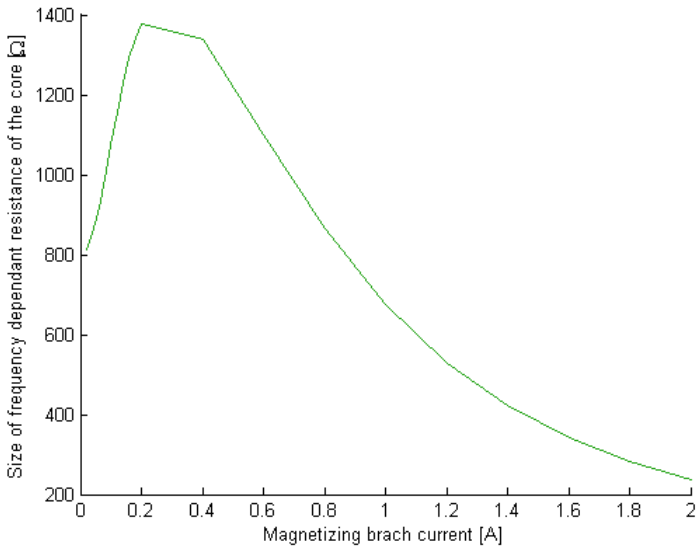

Figure 20: Core resistance R_{core} plotted as function of magnetizing branch current

Leakage inductance is a parameter that is slightly more challenging to estimate correctly using FEMM. One approach is to consider the mutual inductance M and calculate $L_/sigma$ using equation (3.27).

$$L_{sigma} = L_2 - aM \tag{3.27}$$

where L_2 is the self inductance of the secondary winding, a is the coupling coefficient and M the mutual inductance. Mutual inductance of the coils is acquired using equation (3.28).

$$M = L_{mutual} = \frac{n_2}{i_1 a_2}\Big(\int_{J_{2+}} A_1 dV_2 - \int_{J_{2-}} A_1 dV_2\Big) \tag{3.28}$$

where n_2 is number of turns in secondary coil, i_1 current in the primary coil, a_2 the cross section area of the secondary coil, and $\int_{J_{2+}} A_1 dV$ as well as $\int_{J_{2-}} A_1 dV_2$ vector potential integrals over the volume of the secondary coil in the two directions of current flow. The leakage inductance acquired using this method is $1.04\,\mu$H.

Another approach is to calculate the inductances L_{self} and L_{mag} using (3.24) and (3.25) in order to then subtract one from the other in order to acquire L_σ. This gives a value of $1.0\,\mu$H. Notably both values are lower than the leakage inductance suggested by analytic and measurement based estimation. A cause of this is three dimensional nature of the flux leakage, for which FEMM can not account. Both of the acquired values are therefore corrected by a factor of 4 considering the surfaces not accounted for in FEMM. Further estimation method of L_σ is creating conditions corresponding to short circuit, as in short-circuit test, and integrating the stored magnetic energy in the leakage field. The magnetic flux density and flux lines under the mentioned conditions are seen in Figure 21. This method provides a value of $3.45\,\mu H$ after 3D compensation.

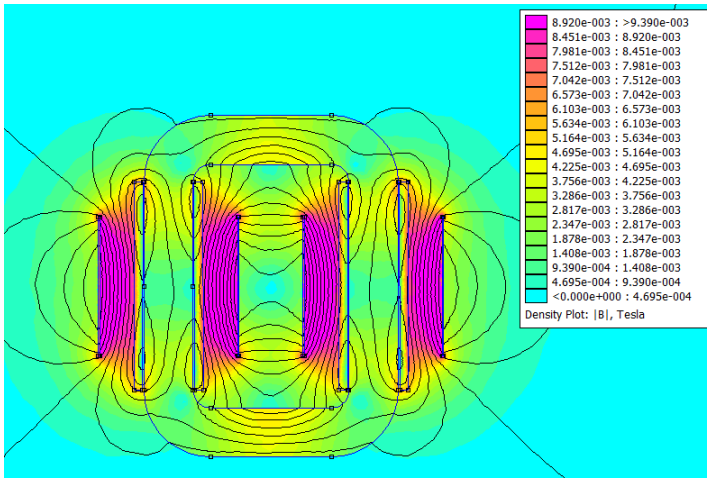

Figure 21: Short-circuit simulation in FEMM

The capacitance values C_{12} and C_{ps} are acquired by using electrostatic mode of FEMM. The model geometry is also changed in order to provide most credible result. The geometry used for capacitance estimation is seen in Figure 22.

The values acquired using the model are $C_{12} = 0.21\,\text{nF}$ and $C_{ps} = 34.0\,\text{pF}$ in air. The values are obtained using integral of stored energy over a region, E_s and equation (3.29).

$$E_s = \frac{CV^2}{2} \tag{3.29}$$

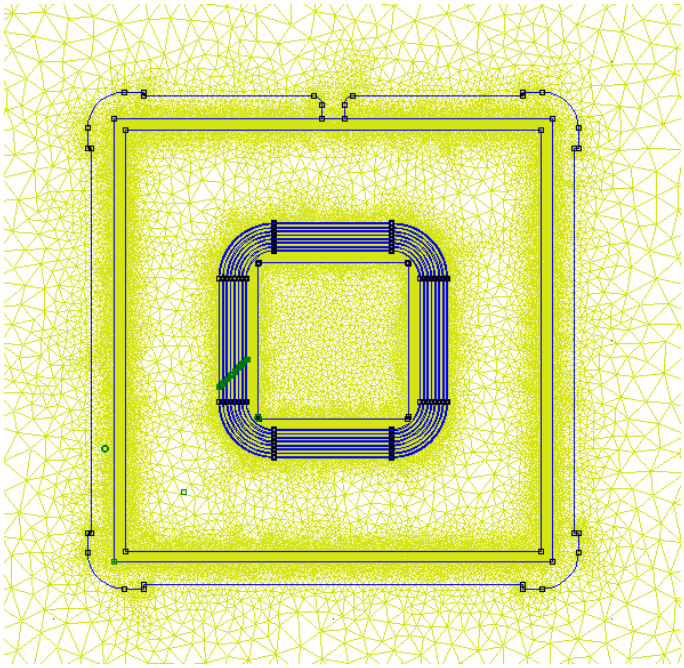

Figure 22: Meshed 2D drawing in FEMM used to calculate capacitive parameters.

Apart from direct equivalent circuit parameters several other interesting results are obtained through simulation in FEMM.

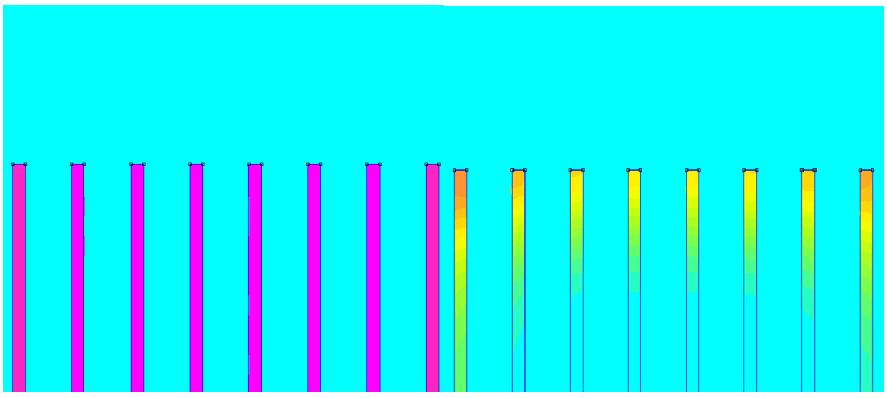

(a) No proximity effect. 0 to 0.0147 MA/m²

(b) Apparent proximity effect. 0 to 0.473 MA/m²

Figure 23: Current density plot in primary winding

The ones related to HV effects are discussed in section 5.1. Aside from these, HF effects in the transformer windings are of interest. In Figure 23 a display of proximity effect is presented.

In figures 23a and 23b the top side of the primary coil is displayed, modeled in FEMM. To the left, in 23a the medium between the winding turns is set to have virtually zero permeability, allowing no magnetic field to be formed. However when air is modeled, as in the right case, Figure 23b, the current density in the primary coil becomes non-uniform ranging from relatively low values to $0.37\,\mathrm{MA/m^2}$. This can be compared to a the uniform value of $0.015\,\mathrm{MA/m^2}$ in the case when turns do not affect each other through induction.

This result is relevant for the value of resistance in primary and secondary winding, where similar effect can be expected to take place. The effective conducting area can be said to drastically decrease as a result of proximity effect. The series resistances of the windings, $R_{1copper}$ and $R_{2copper}$ will thereby rise by a considerable amount.

3.2.5 COMSOL

While FEMM provides excellent functionality for problems which can efficiently be modeled in two dimensions it lacks tools in order to analyze structures which have intrinsically three dimensional nature. This is an area where COMSOL provides many valuable features.

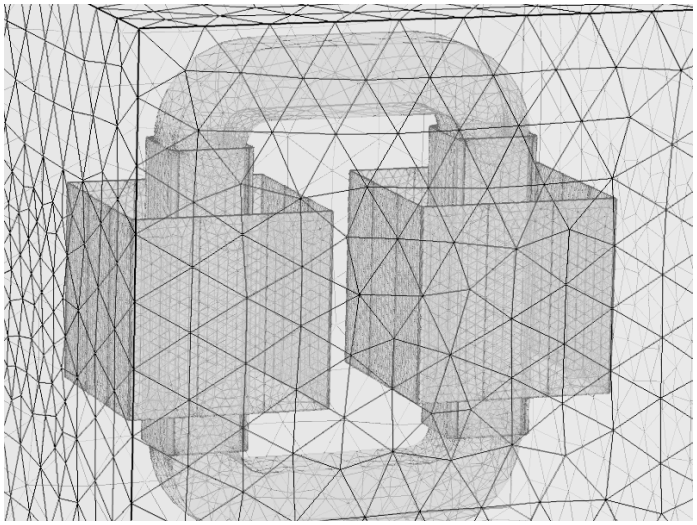

Figure 24: Meshed 3D transformer drawing in COMSOL

For the pulse transformer 2D simulations are sufficient in almost all aspects, due to ability to extrapolate the results to the real three dimensional model without introducing large errors. However in case of some parameters, first and foremost L_{sigma}, the flux leakage between the windings is present in volumes unavailable to model in 2D.

While COMSOL offers a large amount of possibilities and physical studies its computationally demanding and relatively complex program. It is therefore of high value to make the models as small and simple as possible. In picture 24 the transformer, meshed for magnetic testing in COMSOL is shown.

This model, however includes excessively large part of the transformer. Therefore one eight of the design is simulated and the results extrapolated to the full scale design.

L_{mag} is estimated using integration of magnetic flux over the core cross section followed by equation (3.26). The result obtained is 19 mH at 0.5 A magnetizing branch current.

In case of L_σ the parameter is acquired through integration of total flux near center of the coil and at the point furthest away from both windings, by doing this the difference in total flux gives an estimate of the leaked amount. The procedure results in a equivalent circuit leakage inductance of 1.6 μH. The integration is however approximate due to difficulties in integrating stored magnetic energy.

Capacitance calculation is performed through integration of stored electric energy over the region of interest. Resulting C_{ps} is 16 pF. The capacitance C_{12} is not evaluated due to simplistic nature of the transformer model in COMSOL.

The reduced model used for parameter estimation is presented in Figure 25. The resulting simulation outcome from which the parameters are obtained through integration is seen in Figure 26. The windings in the first figure are modeled as solid block with a current and a number of turns assigned to each of them through COMSOL settings. In case of simulation result in Figure 26 the number of assigned turns is four and the current in the coil specified to 0.25 A. The reduction to one eight of the geometry is possible due to symmetrical nature of the transformer, one half, forth or eight of the design can be extrapolated to a complete model, in terms of magnetic properties, without loss of accuracy.

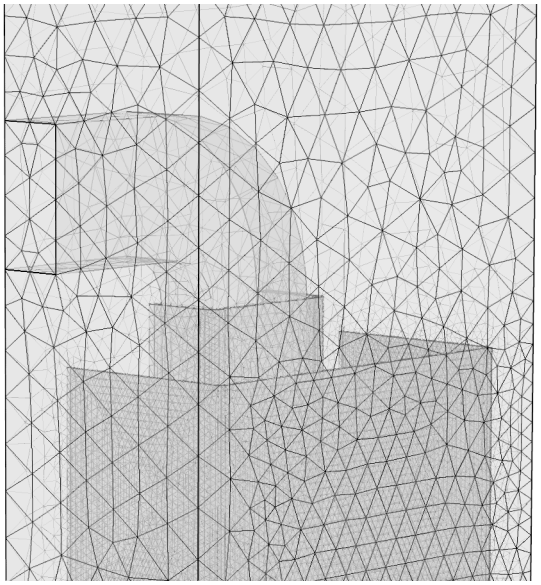

Figure 25: Reduced 3D transformer model in COMSOL with the mesh applied to the design

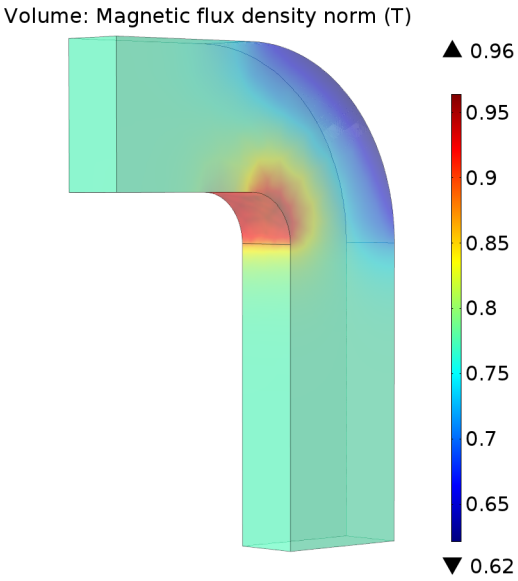

Figure 26: Magnetic flux density plot used to acquire parameters in COMSOL

4 System Analysis

In this chapter the transformer model presented in chapter 3 is subjected to testing. Additionally the transformer and its subsystems are examined together. The tests performed on these configurations are simulation based and primarily examine the square wave response, voltage performance and drops in the system and its resonant behavior.

In order to verify that the results produced by the system simulations are of interest the model results are compared to real tests run on the prototype.

Notably, the equivalent circuit model presented in Figure 6 is to be adjusted in order to undergo system testing. This is due some of the parameters concluded to be insignificant and some needed to be modeled differently due to lack of a transformer equivalent in a real circuit. The new updated model is presented in Figure 27.

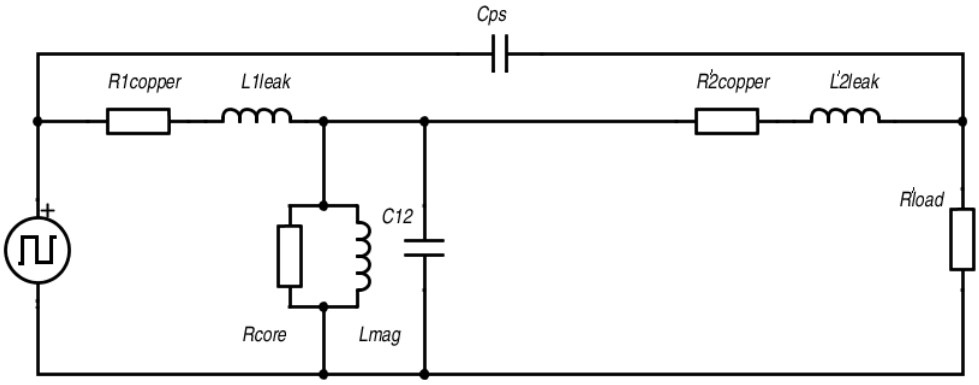

Figure 27: Updated equivalent circuit

The equivalent components from the secondary side have been referred to primary by division with the transformer ratio squared. The referred values are denoted using an apostrophe. It should be noted that the scheme presented is adjusted for simulation purposes and does not strictly represent all requirements imposed by HV criteria, as well as physical details depicted in the original scheme in Figure 6.

Throughout the testing several important principles are employed. First oscillation of each pulse has half of the width of the normal square wave, the measure is implemented due to partially inductive nature of the circuit,

meaning that the current will have an integral component during each cycle. In order to avoid provoking magnetic saturation as well as centering the output current around zero each pulse begins in this specific manner.

The transformer load, R_{load}, is considered to be completely resistive. The nominal load for the transformer unit is 1 kΩ and nominal load current 20 A.

The rise and fall times of the 1 kV 15 kHz input waveform are set to 1μs which is a pessimistic assumption of the real rise and fall times of the switched semiconductor system. Regrettably, no supplier or measurement data is available for these values.

4.1 Transformer Parameter Evaluation

In previous chapter, section 3.2, the means of acquiring equivalent circuit parameters are presented, together with the results they produce. Before proceeding it is however necessary to discuss which of these results are the most useful for modeling the transformer.

Primarily a comparative sanity check is performed, meaning that any parameter varying strongly between the methods are examined. Most of the parameters are in the same order of magnitude and do, at most, vary between the methods by a factor of 3-4. The analytic measurement of capacitance C_{12}, however, exhibits divergent tendency compared to analytic and simulation-based estimation. The cause for this behavior seems to be the resonant nature of the system, resulting in the instruments providing apparent effective values. In case of this parameter, due to relatively simple geometrical shape of the primary winding there are no reasons to assume that analytic calculation or result from FEM analysis are poor estimations. This, in combination with difficulties of analyzing the resonant results provided by LCR-meter suggests that use of the parameter obtained through the other two methods is suitable.

Apparent throughout the thesis is that some parameters behave non-linearly and depend on frequency of applied voltage and magnetic flux density in the core. The frequency dependency is considered of less importance, due to the pulses being of constant frequency at 15 kHz. While including higher frequency components, no frequency changes occur during the operation. The magnetization, however, changes during the pulse, causing permeability to vary throughout each pulsation. This, in turn, results in change of L_{mag} and R_{core}.

These two parameters must thereby be modeled non-linearly in the simulation in order to provide results resembling those during real operation. Such nonlinear parameter estimation is presented for L_{mag} is seen figures 12 and 19. Similar curve is also constructed for the analytic expression (3.7) using the permeability curve in Figure 5 as input. For R_{core} the nonlinear estimation is seen in Figure 20. This behavior of the parameters unfortunately renders virtually useless any singular value acquired at a single operation point.

For the rest of parameters potential minor nonlinear behavior is overlooked, and singular estimations are used as input parameter for the model. Capacitance values for air are used, due to laboratory measurements compared with also being made in air. The values are however easily and quite accurately converted to capacitance in oil through multiplication with ϵ_{oil} = 3.2. This effect is verified by measurement in which a clear increase in capacitance is seen.

4.2 Laboratory Results

Before proceeding with the simulation results several relevant laboratory measurements are presented. Throughout the project a continuous matching procedure is employed in order to acquire most fitting model for the transformer. This procedure is based on comparison of measured values and visual waveforms between real data and simulations.

Several relevant waveforms from laboratory measurements of the transformer prototype are presented in figures 28 through 32. Note that for the first two figures applied square wave has amplitude of 1 kV peak-to-peak despite oscilloscope displaying another value.

In figures 28 and 29 applied voltage of 1 kV square wave can be seen in yellow, current in the primary winding seen in blue and two control signals for the switching logic are seen at the bottoms of the figure.

Clear oscillative behavior can be observed in current waveform following the switch in voltage. The oscillations are observed in the transformer with primary winding constructed using foil coil, . The behavior is explained by resonance phenomena between C_{12} and inductances L_σ and L_{mag} due to high capacitance of the copper foil winding. The results of simulations, discussed in section 4.5, show that the effect is mainly caused by C_{12} and L_σ. The frequency of the oscillation is measured to be approximately 4 MHz.

A display of saturation behavior is shown in Figure 29. Clear current

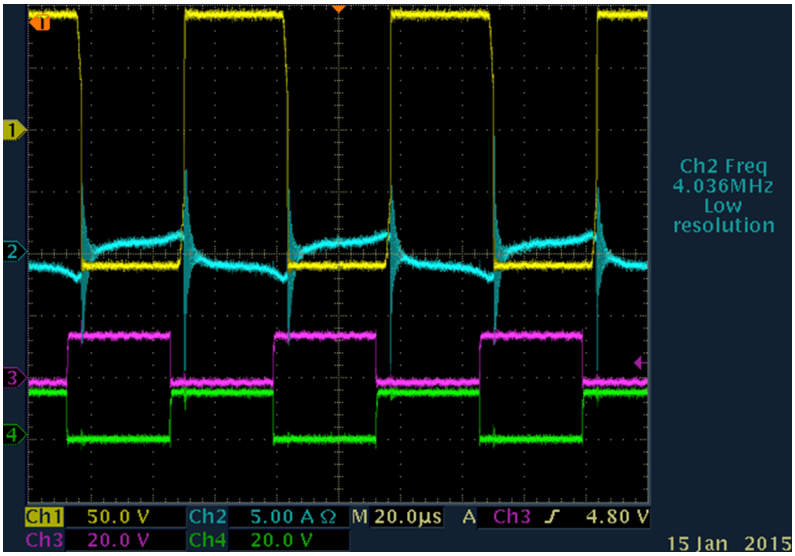

Figure 28: 1 kV, 15 kHz square wave applied to terminals of primary winding without secondary winding attached

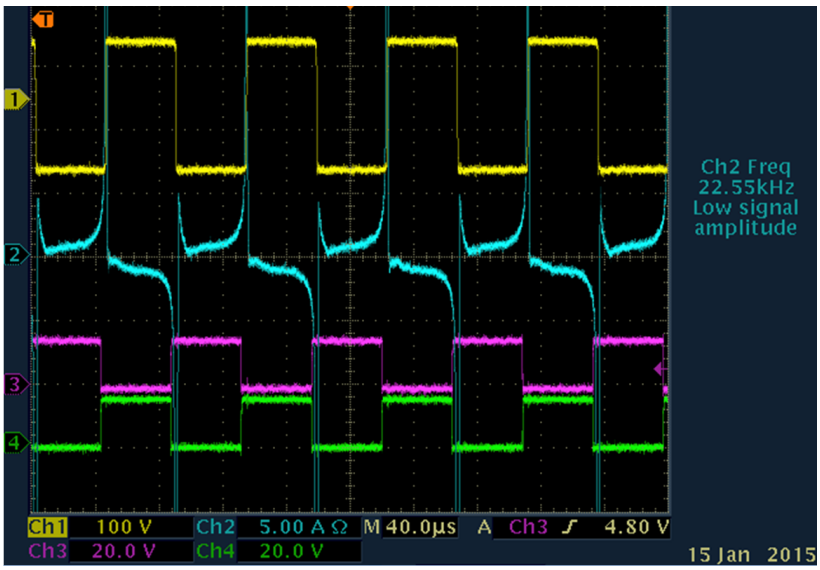

Figure 29: Satururation behavior in pulase transformer

spikes are observed as frequency of the input signal is lowered to 11.3 kHz. This is predicted by equation (3.6). Recurring current spikes are unwanted

due to heating and risk or damaging or burning the primary winding.

In figures 30 and 31 pulse behavior on nominal and high load is shown. In both figures yellow signal represents signal to switching logic, purple the voltage applied to the primary winding, blue the voltage measured over the load and green current through the load.

One may note that oscillations associated with voltage switches are reduced on load due to added branch which can be said to have damping qualities. At 1 kΩ, which is the nominal load for the transformer, the oscillations are very minor.

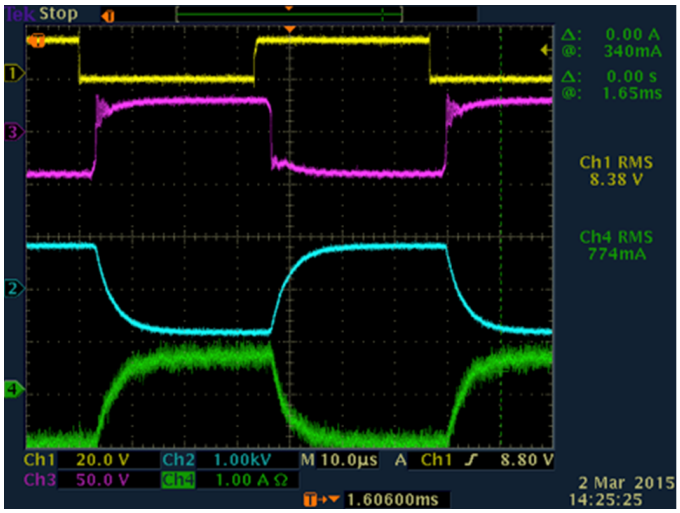

Figure 30: Transformer on load; 40/1000 V with 1 kΩ load

Another effect introduced by the load is the shape of the output voltage. In Figure 30 the blue waveform maintains a soft square shape, in which a series RL-circuit is recognized, formed by $L_{1\sigma}$,$L_{2\sigma}$ and R_{load}. In Figure 31, however, the leakage inductances dominate, forming an almost triangular waveform.

While at the moment of writing the system is not completely assembled, test runs have already been performed on a configuration containing the transformer, the rectifier and a 2300 Ω load. The load, which is lower than the nominal one, results in increased oscillative behavior, but provides a clear idea of how the waveform looks after the rectification. The results of the measurement can be seen in Figure 32.

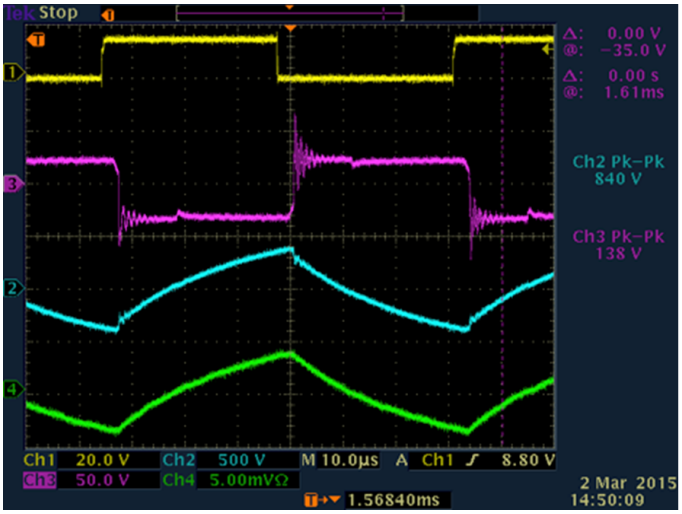

Figure 31: Transformer on load; 40/1000 V with 100Ω load

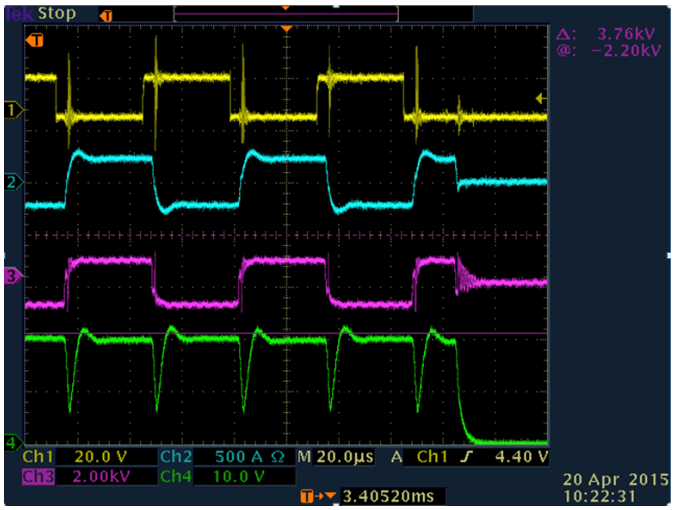

Figure 32: Transformer measurement performed with rectifier and 2300Ω load

In figure 32 yellow signal represents control signal to the switching logic, blue the current in primary winding, purple the voltage in the primary winding and green the voltage over the load. Measurement is performed in oil. Negative voltage spikes due to L_σ are to be noted in the green waveform.

4.3 Square Wave Response

Three simulation tools were used, first one is the software LTSpice, which allows the user to specify a circuit to be simulated and provides among other functions waveform graphs which are however not used in square wave testing. Due to limited possibilities to implement a much needed look-up table for L_{mag} and R_{core} the program is instead run in an iterative manner from MATLAB which updates the parameters with each iteration.

Apart from the LTSpice, Simulink software is also employed for square wave testing. In Simulink two models are constructed, one based on the predefined transformer model and one constructed manually.

Initial choice of parameters is presented in Table 5. Values are selected freely from among the the ones acquired, but represent the value range which most methods confirm.

R1copper	0.24 mΩ
L1leak ($L_{1\sigma}$)	4.5 μH
Rcore	From figure 20 i.e FEMM simulation
Lmag	From figure 19 i.e FEMM simulation
C12	0.25 nF
Cps	34 pF
R2copper	1.5 Ω
L2leak ($L_{2\sigma}$)	2.9 mH

Table 5: Initial parameter selection for square wave test

Test at no load, related to the results in figures 28 and 29 is performed with similar waveform being obtained using all simulation methods. The most relevant similarity is that the waveforms in all simulation enter saturation resulting in current spikes during each period of the square wave. Such behavior at frequency of 15kHz does not agree with the waveform in Figure 28.

It is clear that parameters in the magnetizing branch of the equivalent circuit: L_{mag} and R_{core} are responsible for such behavior and must be manipulated in order to match the laboratory results. An example of saturation in Simulink model is presented in Figure 33. Note that after saturation has occurred the numeric model limits current rise. This means that the most relevant feature of the figure is the onset of saturation. This part of the waveform is comparable to the saturation onset in Figure 29.

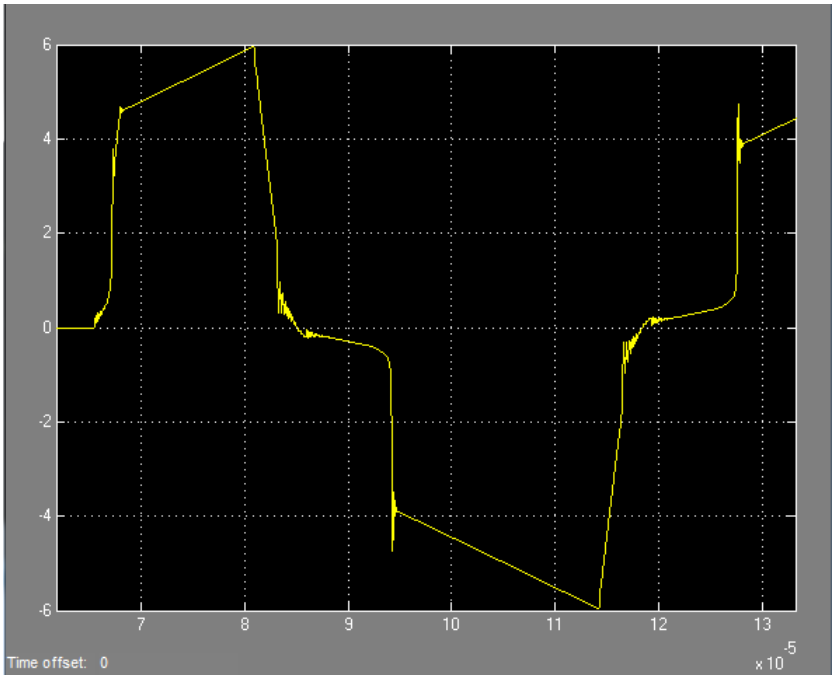

Figure 33: Saturation in Simulink model. Current in [A] on the y-axis.

When L_{mag} and R_{core} are adjusted by a linear scaling factors the results are greatly improved in terms of model matching the reality. The value of the scalar factors determines when and if the saturation region is reached. Adjusting the parameters, however, unavoidably introduces a methodological problem in terms of estimated values of L_{mag} and R_{core} being too small for a nonlinear model accounting for saturation.

Another efficient adjustment to the model is setting R_{core} to a permanent value. An example of such compensation simulated with infinite R_{load} is shown in Figure 34. In fact, predefined transformer model in Simulink does not allow variation of this parameter at all. As seen in the figure the current behavior strongly resembles that of measurement in Figure 28 apart from capacitive tendencies which are much more pronounced in the measurement.

Two other waveforms produced using different compensation constants and methods are attached in Appendix α.

While saturation is a highly important feature in transformer design, it is possible to study outside of equivalent circuit simulation, which drastically simplifies the model. It is therefore often assumed that the parameters

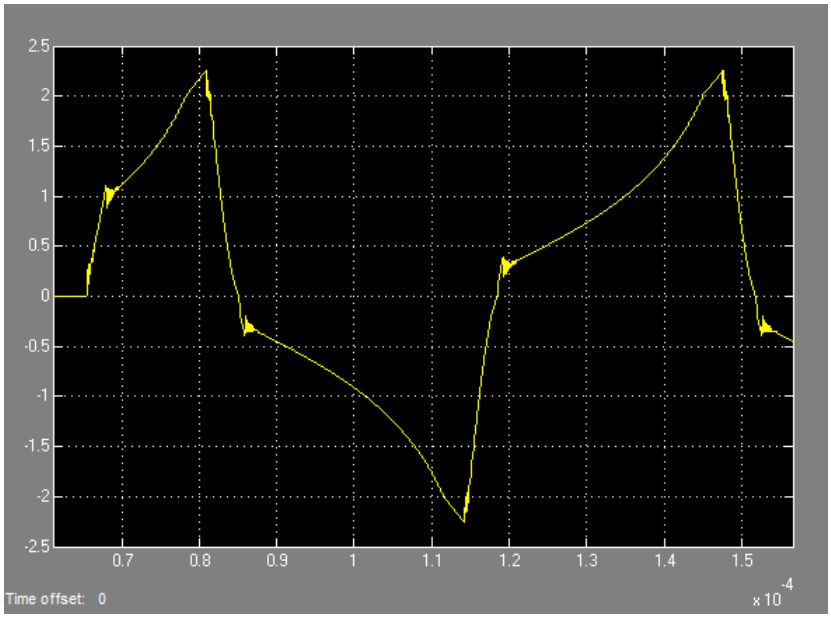

Figure 34: Simulink model with constant $R_{core} = 1100\,\Omega$. Current in [A] on the y-axis.

in the equivalent circuit are modeled as constants [2] [8]. Such model is constructed in LTSpice using parameters in Table 6.

R1copper	$0.24\,\text{m}\Omega$
L1leak ($L_{1\sigma}$)	$4.5\,\mu$H
Rcore	$1100\,\Omega$
Lmag	7 mH
C12	0.25 nF
Cps	34 pF
R2copper	$1.5\,\Omega$
L2leak ($L_{2\sigma}$)	2.9 mH

Table 6: Constant parameter selection for square wave test

Using the presented parameters a series of simulations are carried out at different loads. The simulations are performed using LTSpice and the resulting secondary voltage waveforms for several loads are presented in figures 35a,35b,35c.

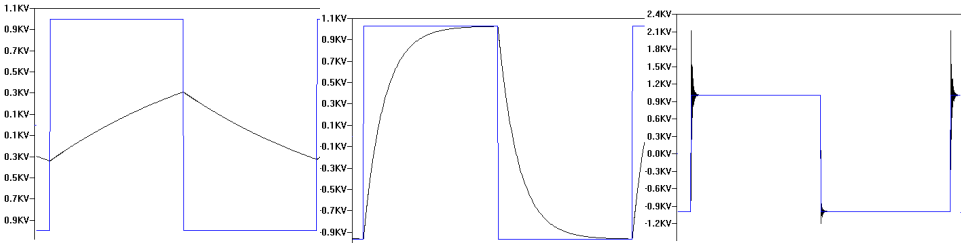

(a) Heavy Load, $R_{load} = 100\,\Omega$ *(b) Nominal Load,* $R_{load} = 1\,k\Omega$ *(c) Light Load,* $R_{load} = 1\,M\Omega$

Figure 35: Voltage over R_{load} *as a result of square wave applied to the terminals or primary winding*

In Figure 35 black waveform represents the 1 kV 15 kHz input voltage to the transformer and the blue waveform the voltage over the load. The three results closely resemble measured waveforms in figures 31, 30 and indirectly Figure 28. A more general idea of response during each flank as a function of load is given by the damping factor in equation (4.1) [16].

$$\sigma = \frac{1}{2R_{load}}\sqrt{\frac{L_\sigma}{C_{12}}} \tag{4.1}$$

If the damping factor σ in equation above is small, typically below 0.6, the pulse response can be expected to have an overshoot and possibly oscillations. The reverse case, where σ is above 0.8 gives a damped square wave response [16].

The results show that equivalent circuit model provides good approximation for the real waveform, even though saturation behavior and nonlinearity of L_{mag} and R_{core} are neglected. In order to account for saturation the current waveform is examined and using magnetization or permeability curve, as well as (3.5) the presence of saturation is deduced.

4.4 On Load and Efficiency Characteristics

Load characteristics are extracted from the equivalent circuit model through LTSpice simulation at a fixed operating point, with the parameters specified

in Table 6. The capacitances C_{ps} and C_{12} are however not included due to their very high impedance value $Z = \frac{1}{j\omega C}$.

A parameter previously not included is the core loss, which is considered to be constant at $P_{core} = 450\,\mathrm{W}$. This value is obtained through FEMM simulation at about 1.8 A, 15 kHz sinusoidal magnetizing branch current and hysteresis lag angle of 0°. The value is low compared to one provided by manufacturer; 675 W at same working point. Both values are however small relative to the input and output power which is measured in hundreds of kW.

Two most relevant results of the analysis is the the voltage drop over the load and efficiency at different loading points.

The voltage drop as function of the load current is presented in Figure 36. The starting and ending points of the curve represent open circuit and short circuit of secondary winding respectively.

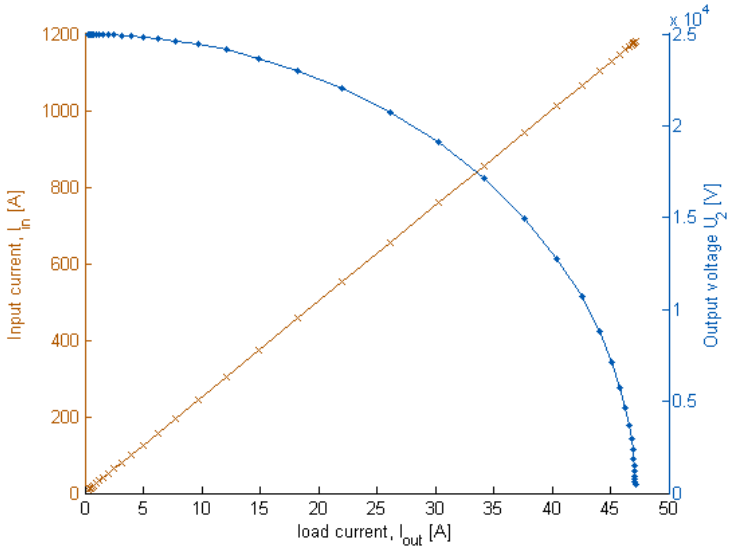

Figure 36: Voltage drop over the load and primary current as function of load current

Simulation result provides an estimation of approximately 1:22.5 voltage ratio over the transformer at 20 A of load current. As the $j\omega$-method used in the simulation it is based on sinusoidal waveforms, which differ from true square wave deviations from reality are expected.

Efficiency of the pulsed transformer is simply calculated through equation (4.2).

$$\eta = \frac{P_{out}}{P_{in}} \tag{4.2}$$

where P_{out} is the real power in the load and P_{in} the real power fed into the system. The resulting efficiency curves acquired through analytic model and LTSpice simulation respectively are presented in Figure 37.

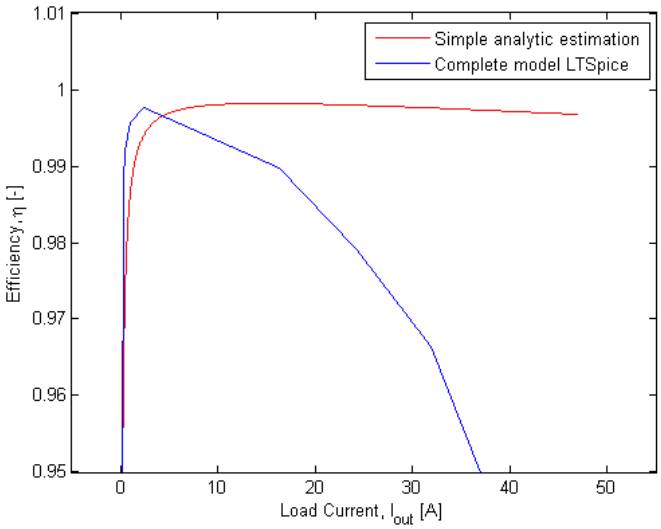

Figure 37: Input power, output power and efficiency as function of load current

As can be seen in the figure the two methods suggest an efficiency of 0.997 and 0.986 at nominal load current of 20 A. The loss of efficiency at higher loading points can be expected due to I^2 factor in equation 3.10 considering copper winding resistances.

Difference in the two results is primarily due to LTSpice using square wave input while analytic method in MATLAB uses $j\omega$ approximation. This results in a highly altering input and output power waveforms in LTSpice at high loads. This behavior is not at all as pronounced in sinusoidal excitation based $j\omega$ method.

The equivalent resistance of the core is considered to be constant in

order to simplify the model. In reality the power lost is dependent on the magnetization branch current and therefore the saturation behavior of the core. The power loss in the core can be said to increase with magnetization branch current and then reach a more or less stable value when saturation behavior becomes apparent. This effect is due all types of core losses being dependent on B, according to (3.9).

4.5 Frequency Sweep

A frequency sweep is performed using LTSpice, which iterates over a chosen range of frequencies and using a small signal model creates a plot of phase and gain of the system or specific components. The obtained waveforms are useful to determine at which frequencies and under which loading conditions resonance phenomena is likely to occur.

This type of analysis is substantial for a pulse transformer due to square wave theoretically containing every odd multiple of its original frequency. The frequency at which the system exhibits resonant peaks will determine the frequency of the oscillation observed after the rise or fall of the pulse. The amplitude of the resonance is related to the gain in the frequency sweep at the frequency of interest.

In figures 38a and 38b frequency sweep over the system can be seen for two different loading conditions. The frequency range analyzed is 1 kHz to 100 MHz.

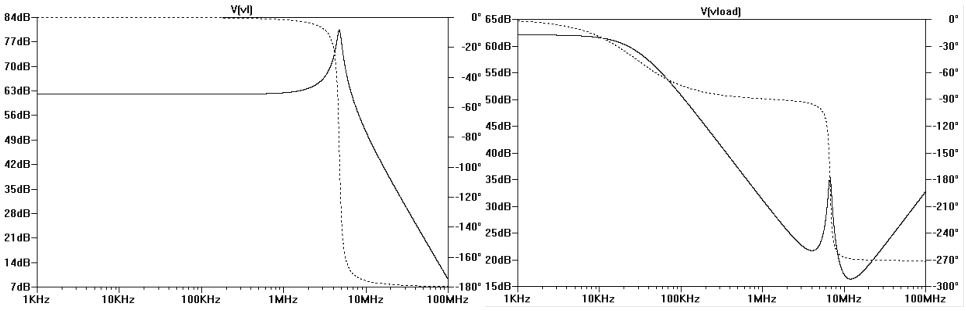

(a) Frequency sweep at no load *(b) Frequency sweep at nominal load*

Figure 38: Frequency sweep for two loading points

In Figure 38a a clear single peak is visible with its center at 4.75 MHz, which agrees relatively well with the frequency measurement presented in section 4.2 attained from the current waveform in Figure 28. The upward

pointing shape of the gain peak suggests that the resonance occurs between two series components, which are represented by L_σ and C_{12} is the equivalent scheme.

The frequency sweep on nominal load, seen in Figure 38b displays a slightly different character. The attenuation starts at lower frequencies and the resonance peak is located at 6.7 MHz resulting in a local gain increase. Due to non-ideal nature of the 1 kV 15 kHz input square wave a large portion of the higher frequency components are missing in the real waveform. This means that early attenuation and shifting the resonance peak higher up in the frequency band makes resonance effects less pronounced.

4.6 Subsystem Characteristics

During the simulations the nominal load of the transformer is considered to be 1 kΩ. In reality, even if the klystron is considered to be a purely resistive, the subsystems separating it from the transformer exhibit a number of nonlinear qualities. These include the diodes in the rectifier as well as saturation behavior in both common mode choke and filter inductor.

While modeling the whole system including the nonlinear behavior is outside of scope of this thesis, parameter and voltage drop estimation is made for the subsystems. Both common mode choke and filter inductor exhibit completely different qualities when subjected to common mode/differential current. The characteristics, achieved through datasheets and parameter acquisition methods described in section 3.2 are partially presented below and partially in Appendix β. The ones presented in this section relate to normal function of the system while those in Appendix β focus on filtering qualities.

Common mode choke has an parasitic, differential self inductance due to flux leakage and winding connection $L_{self} = 33\,\mu$H-$54\,\mu$H and a series resistance of $R_{series} = 0.20\,\Omega$. At nominal current of 20 A a voltage drop of 4 V is present over the resistance.

Ideally common mode chokes have less differential inductance than a usual connection of same length due to cancellation of the magnetic field. However if the windings are placed at different distance from the core room for leakage inductance is introduced due to imperfect symmetry of the installation. Due to the leakage being proportional to N_1^2 according to (3.3) and (3.4) even the small insulation distance separating the windings of the choke can provide non-negligible leakage inductance. In the case of current design, seen from the primary side, the leakage inductance is in the range of 53 nH-86 nH, which is almost factor hundred lower than the transformer

leakage inductance.

Rectifier stack diodes typically have voltage drop associated with each of them. This small drop becomes significant when a large number of diodes are series connected. In the rectifier 22 PCBs with 4 diodes each are used, resulting in a total voltage drop of 70 V at 1 kV. This drop is however likely to slightly increase when nominal voltage of 25 kV is applied. Other parasitic elements of the rectifier can be neglected due to voltage drop over the diodes clearly being the largest source of disturbance.

Notably, the output of the rectifier will not be a completely even dc pulse. As seen in Figure 35b the waveform to be rectified at nominal load will have voltage drops directly related to size of the leakage inductance of the transformer. This effect is displayed in Figure 32

The filter inductor also has a voltage drop associated with it, primarily due to resistance in the 200 turns of copper wire. The total resistance of the windings $R_{series} = 0.98\,\Omega$, results in a voltage drop of 19.6 V at nominal current of 20 A. The inductance of the filter inductor under normal operation is in practice of little relevance due to low frequency of the voltage waveform at 14 Hz 3.5 ms pulse. It is however still useful to take the inductance into account considering its effect on the rise time of the pulse. At nominal current of 20 A the inductance value of the filter inductor is $L_{self} = 58\,\text{mH}$ according to FEMM simulation.

The overall conclusion is that the subsystems have a significant voltage drop over them ranging from around 94V and up to a higher value, depending on character of the diodes used in the rectifier. The total increase should however not exceed several volts. Additionally the subsystems introduce several series inductances along the path of the signal, naturally stray capacitance will also be present. The magnitude of the stray capacitance is however hard to estimate and is left outside the scope of this thesis.

The output voltage waveform is consequently expected to be of lower amplitude than the output of the transformer and also to have increasingly lower rise time at beginning of each pulse. While no measurement result is available for the whole system an idea of the output waveforms is presented in Figure 32.

4.7 Model Accuracy

The model employed throughout the testing is continuously the equivalent circuit model, regardless of if square wave, load or frequency response is the subject of testing. Due to possibility to measure the actual output of the transformer under different conditions the agreement between the model and measurements is possible to verify visually, as in figures 30 and 31, 35a and 35b.

As mentioned the nonlinear modeling agreed to large extent with the laboratory results only after adjustment of the parameters in an iterative manner. This creates doubt regarding the credibility of the equivalent circuit model under nonlinear conditions, but also doubt regarding the acquisition of the parameters for such model. For example equations (3.24), (3.25), (3.26) are only valid under circumstances where no saturation is apparent and preferably in a linear region of the magnetization curve [15]. After the nonlinear modeling is tested a conclusion is made that while equivalent circuit can support this type of model it takes more thorough analysis and numerical modeling in order to get credible results with same pointwise input parameters as for linear model. Linear approximation using equivalent circuit at a specific working point gives excellent approximation of the transformer function aside from the saturation behavior. This, however is based on precise estimation of the equivalent components, achieved through either qualitative or quantitative methods. Results obtained through linear modeling throughout the project are considered to have relatively high accuracy and good agreement with measurements.

There exist several further development possibilities for the accuracy of the model. These are discussed in section 7.1

5 Construction and High Voltage Considerations

The practical part of the project contains a considerable amount of geometrical and mechanical solutions aimed at coping with perilous effects caused by high voltage and imperfection of the materials used in construction of the system.

While not all parasitic effects are taken into account, the ones most relevant are discussed in the following sections.

5.1 Hazards

The hazards discussed can be separated into two main groups. Group one contains effects related to electric fields due to high voltage difference between parts of the system. Group two contains effects related to Joule heating in the system. While both groups are addressed the bigger focus is placed on HV phenomena and the steps taken to prevent it from damaging the system and reducing its functionality.

5.1.1 Corona Effect

Corona Effect is an commonly occurring HV phenomena, seen in power systems within many application. The mechanics behind the effect is acceleration of atoms or gas molecules under high electric field. Corona effect is seen as first step toward electrical arcing.

In air corona is not visible until a certain level of electric field strength is reached, at which point it becomes visible as pale blue or red light surrounding the HV component. Because the mobility of electrons is higher than the mobility of ions, corona discharges occur at lower voltages when the reference potential is lower than the potential of the HV component [17].

The main risks associated with corona effect is power loss, due to acceleration of particles, or in other words currents in proximity with the surface, as well as possible initiation of electrical arcing due to electrons and ionized particles being available in surrounding media.

A risk of degradation of insulation dielectric in proximity to corona discharges also poses as an long term threat [17].

5.1.2 Electrical Arcing

Electrical arcing is a HV phenomena where a high current channel is established through insulating media between two conducting surfaces. The effect

is due ionization of atoms resulting in a conductive route created under high electric field [19].

The phenomena is highly hazardous to both the device causing the arc and surrounding dielectrics, subsystems and equipment. The gases created in mineral oil due to propagation of the arc are combustible and can in worst case lead to fire or explosion [20].

In case of solids dielectrics electrical arcing often causes permanent degradation of the material, leading to impairment of insulation and its mechanical strength. In liquid dielectrics, such as transformer oil degradation is also observed. Typical effects include reduced breakdown voltage, reduced permittivity, introduction of contaminating particles, color change and bubbles in the oil [20] [21]. Most of this effects further increase the risk of new electric arcs, corona effect and drastically decrease the lifetime of the system.

During the HV insulation testing arcing is observed in the transformer prototype. Because the applied voltage is provided by an specially designed instrument the arcing time is very short, with the process being stopped as soon as a significant leakage current is measured. Arcing in oil during the test is displayed in figures 39a and 39b.

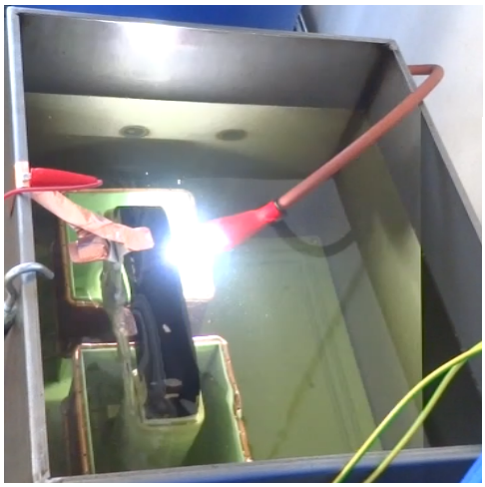

(a) Bright light produced by electric arc seen during prototype test in oil

(b) Two video frames of the arcing phenomena during HV testing in oil

Figure 39: Transformer prototype early HV insulation test

Both arcs in Figure 39 occur between primary and secondary winding when primary is set to ground potential and voltage is applied to secondary. During the early tests the breakdown voltage is around 80 kV.

5.1.3 Thermal Complications

During operation heat is generated in the transformer due to losses in primary, secondary and the core. In the windings the losses are due to Joule heating and in the core due to hysteresis, eddy and anomalous effects. Main problem with heat generation is the danger of reaching temperatures at which dielectric insulation covering the conductors, or being close to the core starts degrading at a significant rate.

Under no load the losses are typically caused by effects in the core and under load to a larger extent by Joule heating in the primary and secondary winding. When a certain temperature is reached the aging of the dielectric accelerates, the temperature in this case is defined by the hottest spot temperature [22].

Highest temperature in the system is typically encountered in the windings. These are insulated from each other and the core by solid dielectric which has a mechanical strength and a dielectric strength. Both of these parameters are lowered as sufficient temperature is reached, making the insulation brittle and potentially releasing water and air in the process [22].

Under extreme circumstances excessive heating poses as a fire risk. Normally, however main cause of fire in transformers is related to gasses released due to arcing in oil. The fire point as well as flash point of transformer oil is typically rather high, in the analyzed case 316°C and 260°C, meaning that fire due to heating in copper wire is relatively unlikely.

In case of ignition of the oil a efficient drainage system is necessary in order to minimize damage to the surrounding equipment [23].

5.2 Protective Measures

In current transformer prototype design several important measures are taken in order to prevent above mentioned negative effects.

During the project these are continuously developed and implemented as new test results show unexpected effects which must be accounted for.

5.2.1 Insulation, Support Structure and Winding Design

Two parameters considered throughout the design of the whole system are creepage distance and clearance distance. Creepage distance refers to dis-

tance between two conductors along a surface while clearance refers to distance through any media separating them, both however specify the minimum distance which prevents electric arcing. The kV/mm ratios are not constant for these parameters and differ with the insulation material and its purity as well as type of voltage applied [24]. The values used as rule of thumb in the design process are 3.75 kV/mm for clearance and 1.36 kV/mm for creepage distance in oil.

To achieve the necessary safety distances between the parts of the system several measures were taken. Components at different potentials are separated by appropriate distances in oil, such as 40 mm between primary and secondary. Further, channels are made in the fiberglass supports in order to increase the creepage path length.

An important detail in construction process is avoidance of any closed conductive loops around the core, in which a considerable current would be induced. Simultaneously the core must be tightly fastened in order to keep correct clearance and creepage distances to other components. Solution implemented in the project is a non-closed aluminum strap pressing the core together with fiberglass plate underneath it.

Wast majority of the support structures are composed out of fiberglass parts both with the function to insulate but also avoid eddy current losses induced in any conducting materials by magnetic fields.

Transformer oil is used in the design both as an insulator, allowing windings to be closer in order to minimize leakage flux but also as a coolant for the system. Additionally liquid dielectric typically recovers better from corona and arcing events due to no permanent channels remaining in the material. A downside of using oil is need for container in which the transformer must be placed, which makes servicing and monitoring of the system a harder task. Inside the container all subsystems must also be compatible with the oil and not produce bubbles of air and gas after immersion. This is the reason for small holes in anti-corona rings. As air has lower electrical permittivity electrical fields will typically be higher in the regions not filled with oil, threatening with corona or arcing [1].

The metallic container containing the oil serves as outer bound for convective heat transfer. At the moment of writing oil circulation is exclusively provided by heat difference and HV effects.

The choice of primary winding has a clear thermal advantage to standard copper wire due to reduction of skin effect and large contact surface

with surrounding oil. As the current passing through the winding will be close to 500 A at nominal secondary current of 20 A the design choice is very important out of a cooling perspective. At 500 A assuming uniform current distribution the current density is $0.7\,\mathrm{A/mm^2}$ which is far below any rule of thumb for for copper conductors. In practice, however, a margin is a good idea due to proximity effect shown in Figure 23b.

5.2.2 Anti Corona/Arcing measures

As the main mechanic responsible for the corona effect and electrical arcing is high electrical field due to high voltage, the most important measure in order to reduce or abolish the effects is to reduce the field strength. Because reducing the 115 kV voltage needed for the klystron is not a valid option, another approach is necessary.

It is known that sharp edges of conducting materials are prone to having a high electric field around them [1] [18]. This effect is shown through FEMM simulation in figures 40 and 41.

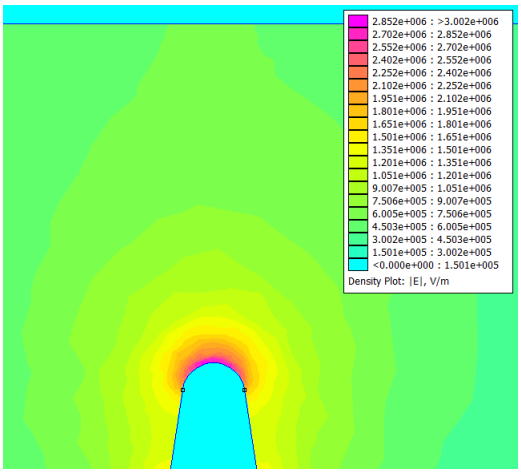

Figure 40: Blunt HV needle directed towards a ground plane

Figures show a setup containing a HV "needle" at a potential of 100 kV and a ground plane, 17.5 cm away at 0 V. As seen in the the figures the maximal electric field is reduced by a factor of 5 when the radius of the needle edge is increased from 0.1 mm to 0.4 mm but remains at same distance form the plane. Consequently the main method of decreasing the electric field in order to avoid the unwanted effects is to increase any edge radius or

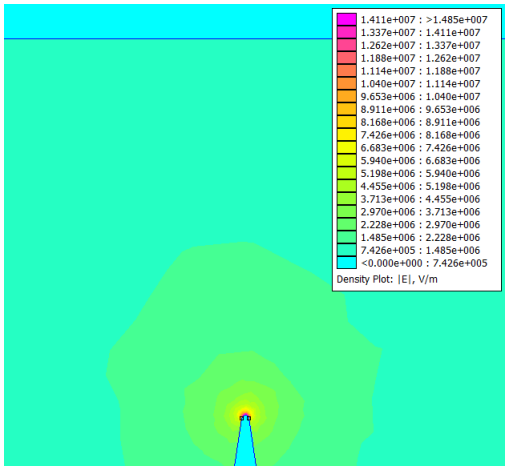

Figure 41: Sharp HV needle directed towards a ground plane

surface area which could be prone to generating high electrical field.

Another method is increasing distance between components with large voltage difference, which also reduces the electric field [24].This is however undesirable due to spatial constraints and increased flux leakage between windings. The solution is implemented to a certain degree through clearance and creepage distance measures.

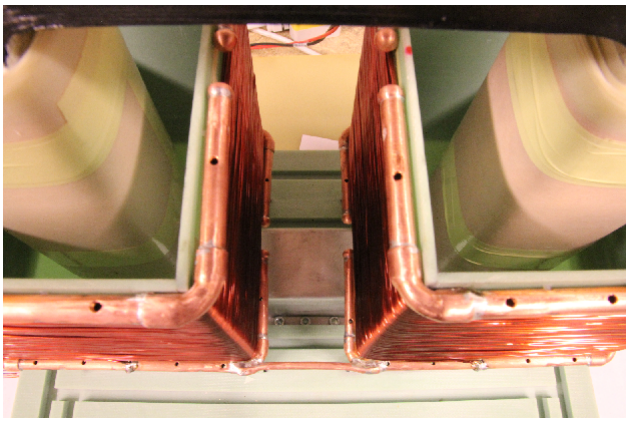

Figure 42: Anti-corona rings implemented on the secondary of the prototype transformer

In order to provide blunt edges for components in the system anti-corona rings are implemented. These are hollow copper pipes with a diameter

around 10 mm which are connected to conductive parts of the system such as first and last turns of the windings of the transformer, common mode choke and filter inductor. Anti-corona rings mounted on secondary winding of the transformer are seen in Figure 42.

As seen in Figure 2 anti-corona rings also run along the otherwise sharp edges of the rectifier PCBs. Where anti-corona rings can not be fitted the edges of the conductors are either placed at suitable distance from surrounding potentials and/or are rasped and shaped to reduce electric field along the edges.

A simulation of the electric fields for the transformer core is performed in FEMM due to highest voltage difference at closest range being found between primary and secondary winding of the transformer. The result of simulation can be seen in Figure 43.

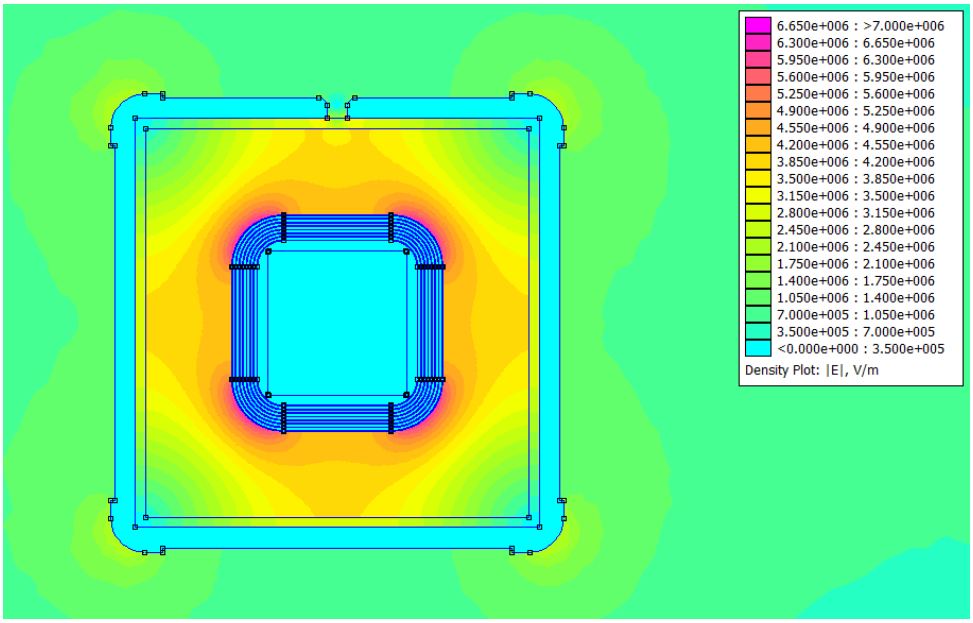

Figure 43: FEMM simulation of the electric field in the cross section of the transformer

In the figure secondary winding and anti-corona rings are set to a potential of 150 kV while primary winding is set to 0V. Electrical field intensity is observed to be highest along the curvatures of the geometry with local values at around 7 MV/m.

The breakdown voltage of air is 3MV/m which means that the transformer could not be operated without an stronger dielectric separating the windings. Transformer oil used has a breakdown voltage of approximately 12 MV/m which is sufficient under optimal conditions [1]. As the oil absorbs moisture and becomes contaminated with particles and bubbles during testing and usage, and as undetected scratches and edges might exist in the prototype, the limit is easily surpassed. This is apparent in Figure 39.

5.3 Miscellaneous Observations

During HV testing an interesting effect is observed in the transformer oil. Namely, when a component is set to a high electric potential, without conducting any electrical current, the oil around the part starts flowing seemingly in direction from the component. The behavior, unexpected in a dielectric could be explained by space charge being generated in oil surrounding the component and then repelled by the electric field.

The effect could be put to good use under operation if the movement of oil is sufficient to considerably increase the convection heat transfer and thereby cool the transformer.

An unrelated mechanical problem is the outer layer of the transformer cores. Testing have shown that nanocrystalline material of the cores is covered by a single layer of dielectric. This cover is prone to crumble when mechanical stress is applied, releasing particles into the transformer oil and uncovering the core material which further contaminates the oil with small conductive particles.

As discussed earlier, contamination of oil could severely reduce its breakdown voltage. The implemented solution is, as mentioned in 2.2.1 two layers of epoxy and one layer of transformer tape covering the whole surface of the core.

6 Evaluation of Current Design

In this chapter the results of evaluation are discussed and possible alterations of the transformer system design are proposed.

6.1 Meeting Requirements

The output voltage amplitude requirement on each subsystem is $\frac{115}{6} = 19.2\,\text{kV}$ while the output voltage at nominal load current is 22.4 kV according to simulation. The result is however based on simulations conducted using sinusoidal exitation. In reality response to each square waveform will have a rise time due to leakage inductance, meaning that the voltage rms value out of the system will be lower than than the expected 25 kV. A simple estimation of this effect can be done using the leakage inductance of the primary and secondary winding at the nominal loading point of 500 A of primary current and 1 kV of primary voltage. The equation used is one defining the voltage drop over inductance and is seen in (6.1) [1].

$$v(t) = L\frac{di}{dt} \tag{6.1}$$

The equation suggests that the time it takes for the pulse to go from peak to peak is $9\,\mu$s. With a period duration of $6.67\,\mu$s this would mean that the transformed waveform will be at maximum value only 73% of the pulse. The maximum voltage value is defined by voltage drop over the winding resistances and the subsystem voltage drops. In practice, within the time between the stable voltage levels the current fed from the source is very low, resulting in a overall loss of power during the rise of each flank. This can be modeled as complete voltage loss during 27% of the pulse, resulting in an average output of 18.3 kV. After subtracting the subsystem voltage drop the output value becomes 18.2 kV resulting in a total voltage of 109 kV. This result is however highly dependent on estimation of leakage inductance meaning that the accuracy is as precise as the acquired value of the parameter. In above calculation a value of $4.5\,\mu$H is used.

Both results are below the theoretical output of 25 kV, as expected, but are close to the specified 19.2 kV per transformer unit. The second estimation does display tendencies toward worryingly low output voltage due to leakage inductance.

During the testing at no load, saturation behavior is at the brink of appearance and is easily provoked by bad symmetry of the input signal or slight erroneous offset. This can be a troublesome tendency if the transformer is operated outside the nominal and high load region.

The rise time of the output pulse does not give any reason to concern, even with pessimistic prognosis regarding the parasitic inductance of the subsystems the transformer unit should be able to produce pulses with rise time well below 100 μs.

The oscillations caused by resonance in the system are pronounced at low and no load. At nominal load these are heavily damped and do not imply negative consequences for the system functioning. This means that the behavior should not be a problem during normal operation.

Additionally, klystrons are in reality not completely resistive loads, but have an additional capacitance which makes them a more damping load then expected [16]. This means that overshoot and slight oscillations in the output are likely not to be a problem.

Layout of the system is carefully designed with appropriate clearance and creepage distances and solid fiberglass support structure. Simultaneously every subsystem and transformer part are kept at closest allowable distance making the design very volume-efficient.

6.2 Improvements and Alternative Designs

Conventionally two types of transformer geometries are the most used; core and shell type [3]. In HV applications core type transformers are superior due to lighter and more compact core, smaller volume due to insulation requirements and more exposed windings, which is important for efficient cooling. While still left with similar core shape, a number of options are available when it comes to winding arrangement, core cross section and number of turns per winding.

During the evaluation and testing the most troublesome tendency of the current design is relatively high loss of voltage due to large leakage inductance and secondarily the bothering proximity to saturation towards the end of each pulse. Drastic variation of the output voltage over the nominal load for several leakage inductances is shown in Figure 44.

The two issues are related through several parameters, but most noticeably the number of turns in the windings, according to equations (3.3),

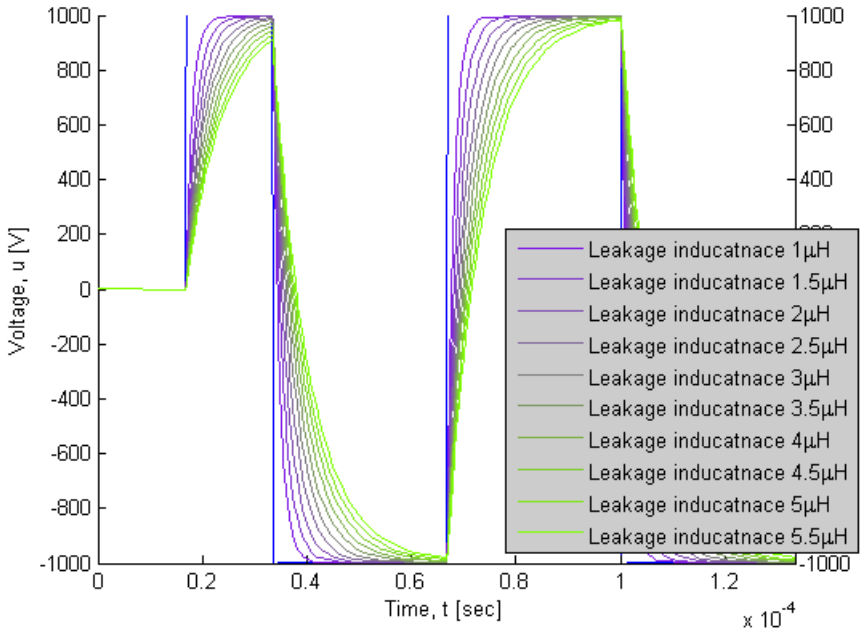

Figure 44: Output voltage over the load for several values of leakage inductance

(3.4), (3.5) and (3.6). By reducing N of both primary and secondary side both the saturation and leakage inductance is decreased. However, in order to maintain approximate total magnetic flux, Φ_B, another parameter needs to compensate for the reduction of N. A possible choice of parameter is A_{Fe}. A planned modification for the transformer is therefore a doubling of the core cross section, by adding another identical core in parallel with the fist one. This allows for a reduction of primary turns up to four as $\Phi_B \propto NA_{Fe}$. Self inductance of the configuration should however maintain approximately same value, resulting in a reduction of turns by 2, according to equation (3.7).

The value of leakage inductance for several other configurations is extrapolated from the parameter estimation and seen in Figure 45. Notably the leakage inductance increases with number of cores due to increasing area between the primary and secondary windings when a new core is added.

Apart from lowering the number of turns, other strategy is also applicable in order to further reduce the leakage inductance. The area between primary and secondary is then to be reduced as follows from (3.3) and (3.4).

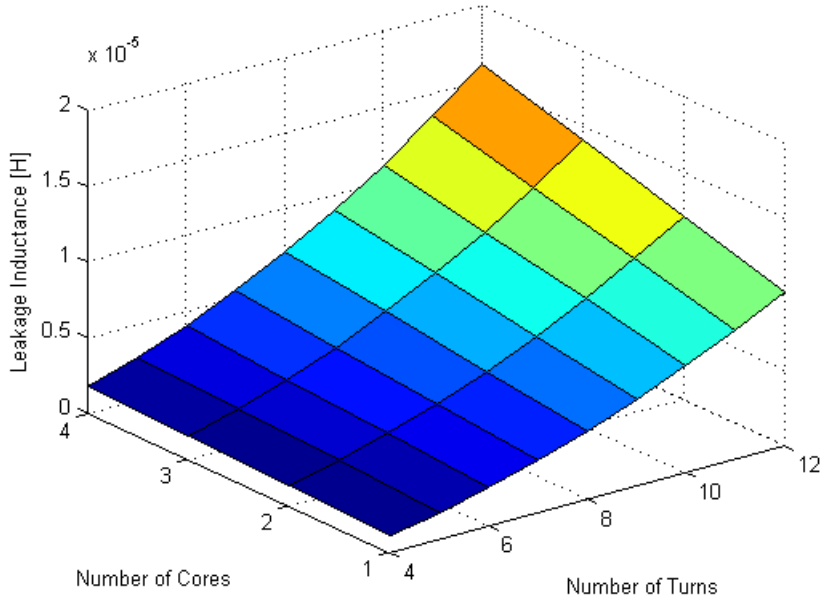

Figure 45: Leakage inductance as function of number of cores and primary turns

A feasible strategy is to simply shorten the insulation distance between the windings as far as creepage and clearance requirements are fulfilled. This can be performed gradually for each series coupled transformer. Such solution, however, leads to different designs for transformers withing the same system, implying constructional and maintenance difficulties. Simultaneously, the importance of reducing L_σ is very high, as displayed in Figure 44, meaning that that such solution is still to be considered.

Final look into the leakage inductance equations presents an option of increasing the core window height further and making both primary and secondary winding increasingly higher. Such solution is to a certain degree limited by the need of keeping l_{fe} constant, if other parameters are to remain unchanged.

If tests on real load or an equivalent show that the resonance caused by L_σ and C_{12} is causing problems a solution to this can be reducing the value of C_{12}, in accordance with (4.1). This can be done by changing the type of primary winding to one with less capacitance between each turn, such as wire, this however would result in an drastic increase if flux leakage. A

more careful solution would be to insulate each turn of the copper foil with low permeability insulator and pack the turns tightly enough to prevent the oil from filling any unoccupied gaps. This would reduce the capacitance according to (3.11) based on that the distance between the turns is already very small.

A constructional improvement reducing the amount of particles in the oil as well as increasing the mechanical stability of the structure and windings is applying transformer lacquer to whole core. At the moment this is done with layers of epoxy. While transformer lacquer could prove to have better result it requires drying in high temperature around 100°C.

During HV testing flashovers occurred between primary and corona ring of the secondary. While the clearance distance between the two is sufficient, attention should be paid to any curvature, edge or scratch which can increase the electric field beyond the dielectric strength of the oil. While electrostatic simulations can be carried out in order to get an idea of the weak points of the design a manual examination should always be performed for each HV transformer and subsystem. If small radii are found they must be covered over with conductive tape, solder or other conductive media or smoothed out.

If the measures are proven to be insufficient anti-corona rings, or conductive caps with a large radius should replace the old ones in order to further reduce the electric field.

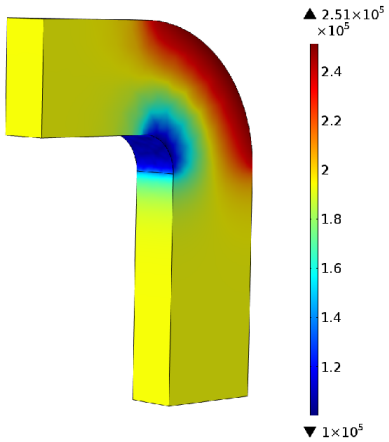

Figure 46: Permeability plot in the 3D transformer model

An interesting result received from COMSOL simulation is the permeability distribution in magnetized core, which is seen in Figure 46. The result suggests that the outer bends of the core are under-utilized as flux path, meaning that if outer section could be compressed, or altered, volume of the core would be reduced without changing its magnetic qualities. Naturally this is a question of manufacturing complicity and cost.

7 Further Work

While performed analysis covers most of the basic functioning of the transformer, several additions to the current model, as well as completely new physical models can be implemented. These are then to be verified by a set of new measured lab data.

7.1 Excluded Circuit Components

The circuit model itself can be further developed in order to achieve a better representation of the physical processes ongoing in the transformer. Such elaborations include giving separate components to each turn of the primary, and if desired, secondary winding. Apart from distributing already existing ones currently excluded parameters, specifically C_{11},C_{21} and C_{22} are to be added to the equivalent circuit model.

7.2 Excluded Physical Phenomena

Currently no thermal model is constructed for the transformer, as well as void of data regarding temperature, cooling and heat transfer. While precautions are taken in order to avoid excessive heating it is useful to be able to predict the temperatures in the system, hot spots and thereby be able to predict the degradation rate of dielectrics and life expectancy of the system.

Thermal analysis could also be proven to be useful when looking a nonlinear behavior of equivalent circuit components as a function of temperature.

Electrostatic phenomena for the subsystems and the assembled transformer system is currently not considered. While working with high voltages a large amount of valuable information about high electric fields can be obtained from a full scale electrostatic model.

Proximity and skin effect are considered throughout the work, but are being regarded as negligible due to voltage drop over winding resistance being insignificant compared to the voltage difference over leakage inductance. Effective resistance values for multiple winding configurations could be very relevant if geometry allows significant skin or proximity effect.

While not being at the center of attention due to lack of moving parts, mechanical stress model can provide some much valuable information on

effects of high currents on transformer windings. As with other physical phenomena this can be modeled in different ways, an analytic model of mechanical stress due to external short circuit is presented in following article; "Transformer mechanical stress caused by external short-circuit: a time domain approach", A. C. de Azevedo et al. (International Conference on Power Systems Transients).

7.3 Full Scale Model

Given a considerable amount of time and resources a full scale equivalent circuit model, including temperature dependence as well as saturation dependence could be constructed for the transformer and the subsystems. Such model could then be subjected to iterative testing through simulation in order to provide a forecast regarding parameters for a sought system.

Such model could also include a thorough representation of the 1 kV voltage source and of the load klystron.

More realistic approach is however to create smaller, simplistic models for the transformer prototype with reasonable alterations of several design parameters. Such parameters could be number of, or cross section area of cores with different permeability, number of primary and secondary windings or their geometry.

8 References

References

[1] "Physics for Scientists and Engineers", Paul A. Tipler, Gene Mosca, 2008

[2] "Electrical Machines", J. Hindmarsh, 1965

[3] "Electric Machines", Mulukutla S. Sarma, 1985

[4] "More Precise Model for Parasitic Capacitances in High-frequency Transformer", Mao Xinkui, Chen Wei, Electrical Engineering Department, Fuzhou University, 2002

[5] G. Ortiz, J. Biela, J. W. Kolar, "Optimized Design of Medium Frequency Transformers with High Isolation Requirements", Power Electronic System Laboratory, ETH Zurich, 2010

[6] Vacuumschmelze, Nanocrystaline Vitroperm EMC products

[7] "Photonic Crystals, Toward Nanoscale Photonic Devices", Jean-Michel Lourtioz Et.al, Springer, Berlin, 2005

[8] "Electrical Machines", Chandur Sadarangani, 2000

[9] "Analysis of electromagnetism in a single-phase transformer", Avo Reinap, $http://www.iea.lth.se/emk/exercises/EMK_task_2.pdf$

[10] "Formelsamling Elektromagnetisk Fltteori", Institutionen fr elektrovetenskap, LTH, 2002

[11] "Anomalous Loss Hysteresis Loop", Adriano A. Almeida, Daniel L. Rodrigues-Jr, Laura S. P. Perassa, Jeanete Leicht, Fernando J. G. Landgraf, 2014

[12] "Predicting iron losses in soft magnetic materials with arbitrary voltage supply: an engineering approach", A. Boglietti, A. Cavagnino, M. Lazzari, M. Pastorelli, 2003

[13] "Electromagnetic transformer modelling including the ferromagnetic core", David Ribbenfjrd, 2010

[14] "Measurement of complex permeability of magnetic materials", V. Dumbrava, L. Svilainis, Department of Signal Processing, Kaunas University of Technology 2006

[15] "Finite Element Method Magnetics, Version 4.2, Users Manual", David Meeker, 2010

[16] "Design procedure for compact pulse transformers with rectangular pulse shape and fast rise times", D. Bortis, J. Biela, G. Ortiz, J.W. Kolar, 2010

[17] "Corona and Arcing in Power and RF Devices", Dheena Moongilan, 2009

[18] "Simulation of the electric field strength in the vicinity of metallization edges on dielectric substrates", C.F. Bayer, 2015

[19] "The electric arc and its function in the new welding processes", P Alexander, 2013

[20] "Effects of Electric Arc on The Dielectric Properties of Liquid Dielectrics", Suwarno and F. Salim, 2008

[21] "The Study of The Arcing Phenomena of The Mineral Oil Using The Rod - Plane Electrode Configuration", N. Pattanadech, F. Pratomosiwi, B. Wieser, M. Muhr, M. Baur, 2012

[22] "Fundamental principles of transformer thermal loading and protection", J. Perez, 2010

[23] "Passive Fire Protection for Major Transformers", W.J. Bronkhorst, 1992

[24] "High Voltage Engineering, Practice and Theory", J.P. Holtzhausen, W.L. Vosloo

9 Appendix α

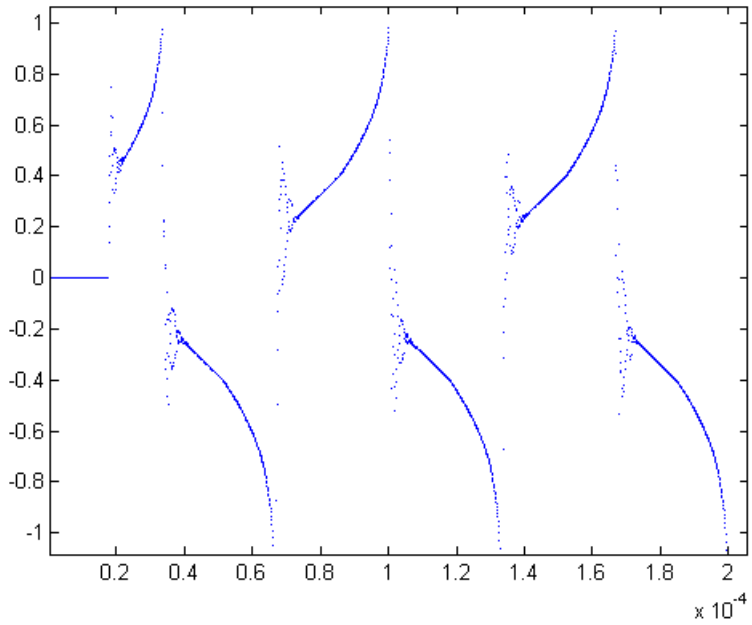

Figure 47: Nonlinear model square wave current response using LTSpice/MATLAB

In Figure 47 a simulation result is shown for square wave response using LTSpice controlled from MATLAB. MATLAB is in this case used as look-up table for the parameters L_{mag} and R_{core} which are both adjusted by a factor of 1.9. Rest of parameters used in the simulations are shown in Table 7. Because the result is acquired pointwise the oscillations as result of each flank are displayed as disconnected points.

R1copper	0.24 mΩ
L1leak ($L_{1\sigma}$)	4.5 μH
Rcore	From Figure 20 i.e FEMM simulation
Lmag	From Figure 19 i.e FEMM simulation
C12	0.25 nF

Table 7: Constant parameter selection for square wave test

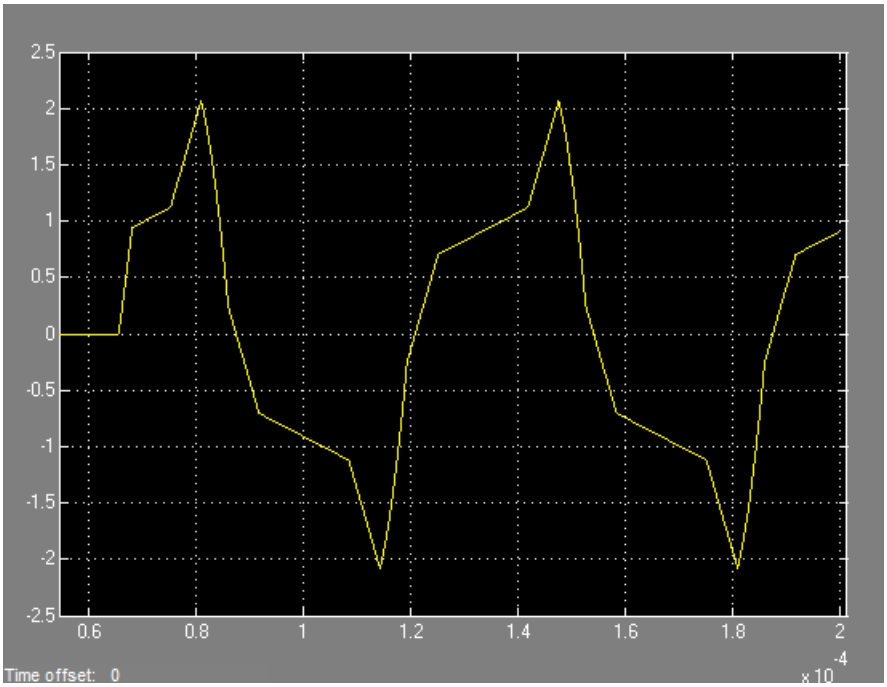

Figure 48: Nonlinear model square wave current response using predefined saturable transformer model in Simulink

The waveform displayed in Figure 48 is acquired using a predefined model in Simulink which requires current-flux points and a constant R_{core} value as input. The flux points were extracted from FEMM simulation of L_{mag}. The constant R_{core} value used is $1100\,\Omega$, the flux values were multiplied by a factor 5 if order to give result similar to reality in terms of magnitude.

The results of all nonlinear simulations continuously resulted in pronounced saturation and high current levels. This is supported by the fact that the current design shows tendencies of saturation during measurements at no load. However it is highly probable that the results extracted through FEMM in combination with the numerical methods provide poor model for real saturation.

10 Appendix β

Figure 49 shows the common mode inductance of the common mode choke and Figure 50 shows differential mode inductance of the filter inductor.

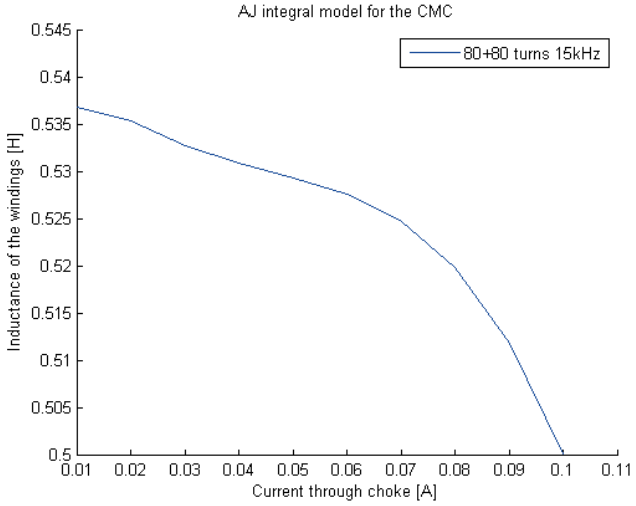

Figure 49: Common mode inductance as function of current through the CMC

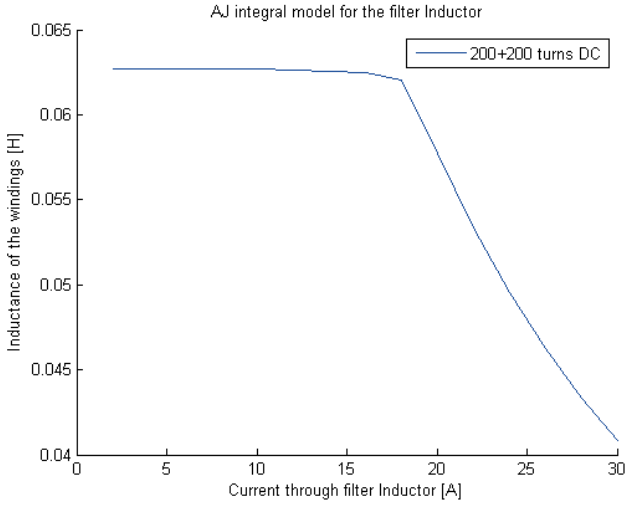

Figure 50: Differential mode inductance as function of current through the filter inductor

11 Appendix γ

Figures 51, 52, 53 and 54 show implemented transformer models in LTSpice and Simulink. In Figure 51 the equivalent circuit at nominal load is shown, implemented in LTSpice, with constant magnetization branch parameters.

Figure 52 shows the framework for nonlinear equivalent circuit model at no load, implemented in Simulink in order to include saturation behavior into the analysis. Figure 53 shows the Simulink block containing the lookup tables for the nonlinear magnetization branch parameters as well as capacitance C_{12} and leakage inductance implemented using integral and derivative blocks in Simulink.

Figure 54 shows predefined, no-load transformer model in Simulink, where input parameters are assigned through a current/magnetic flux pairs and a constant R_{core} value.

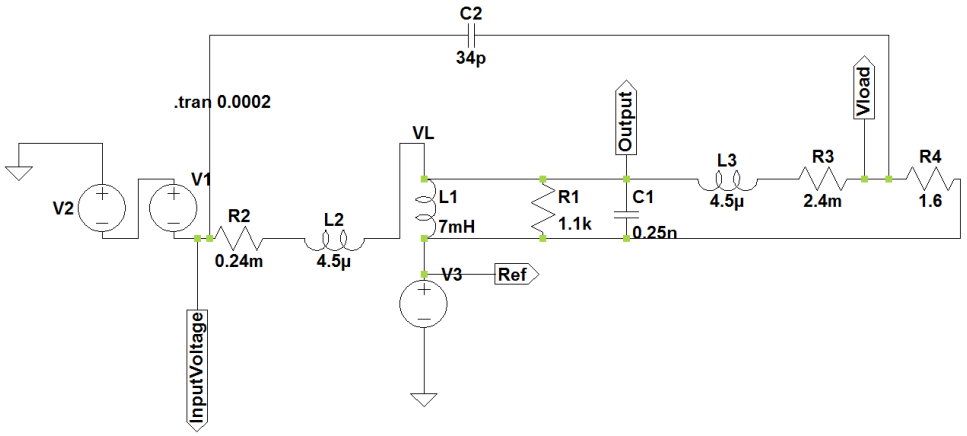

Figure 51: Equivalent circuit model implemented in LTSpice

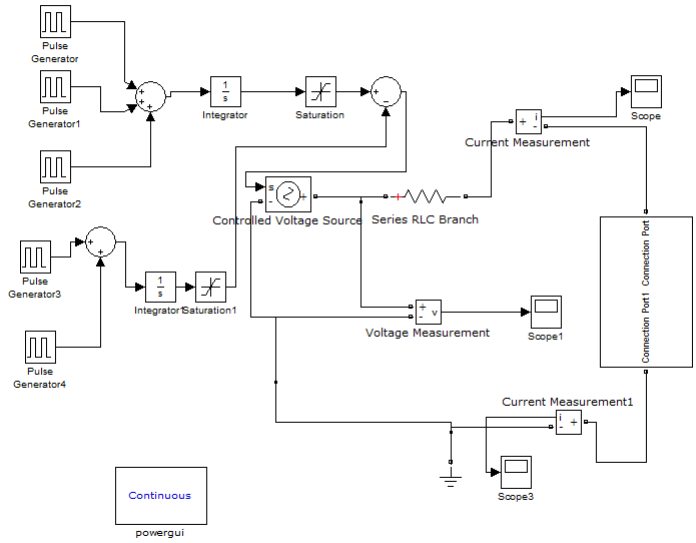

Figure 52: Part 1 of the nonlinear equivalent circuit model in Simulink

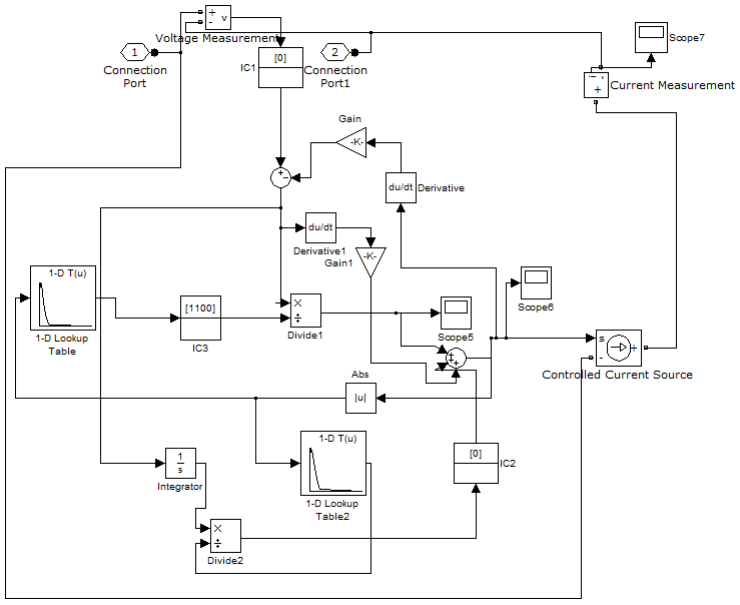

Figure 53: Part 2 of the nonlinear equivalent circuit model in Simulink

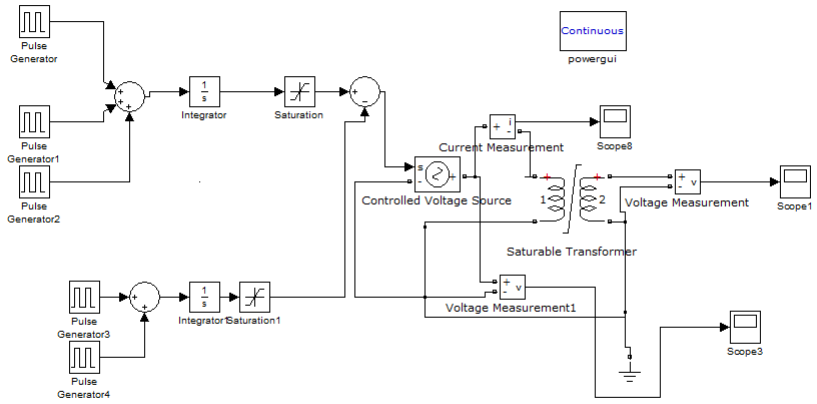

Figure 54: Nonlinear, predefined transformer model in Simulink